

**Understanding  
of  
Materials State and its Degradation  
using  
Non-Linear Ultrasound (NLU) Approaches**

**Submitted to  
AOARD  
AFOSR  
Tokyo, Japan**

**Principal Investigator  
Dr. Krishnan Balasubramaniam  
Department of Mechanical Engineering and  
Centre for Nondestructive Evaluation  
Indian Institute of Technology Madras, Chennai, 600 036  
Tele: +91-44-2257-4662  
Fax: +91-44-2257-0545  
Email: [balas@iitm.ac.in](mailto:balas@iitm.ac.in)**

**Jan 2011**



Report Documentation Page		Form Approved OMB No. 0704-0188
Public reporting burden for the collection of information is estimated to average 1 hour per response, including the time for reviewing instructions, searching existing data sources, gathering and maintaining the data needed, and completing and reviewing the collection of information. Send comments regarding this burden estimate or any other aspect of this collection of information, including suggestions for reducing this burden, to Washington Headquarters Services, Directorate for Information Operations and Reports, 1215 Jefferson Davis Highway, Suite 1204, Arlington VA 22202-4302. Respondents should be aware that notwithstanding any other provision of law, no person shall be subject to a penalty for failing to comply with a collection of information if it does not display a currently valid OMB control number.		
1. REPORT DATE <b>08 FEB 2011</b>	2. REPORT TYPE <b>Final</b>	3. DATES COVERED <b>18-06-2009 to 18-07-2010</b>
4. TITLE AND SUBTITLE <b>Understanding of Materials State and its Degradation using Nonlinear-Ultrasound (NLU) Approaches</b>		5a. CONTRACT NUMBER <b>FA23860914129</b>
		5b. GRANT NUMBER
		5c. PROGRAM ELEMENT NUMBER
6. AUTHOR(S) <b>Krishnan Balasubramaniam</b>		5d. PROJECT NUMBER
		5e. TASK NUMBER
		5f. WORK UNIT NUMBER
7. PERFORMING ORGANIZATION NAME(S) AND ADDRESS(ES) <b>IIT Madras,Center for Non Destructive Evaluation,Chennai 600036,India,NA,NA</b>		8. PERFORMING ORGANIZATION REPORT NUMBER <b>N/A</b>
9. SPONSORING/MONITORING AGENCY NAME(S) AND ADDRESS(ES) <b>AOARD, UNIT 45002, APO, AP, 96338-5002</b>		10. SPONSOR/MONITOR'S ACRONYM(S) <b>AOARD</b>
		11. SPONSOR/MONITOR'S REPORT NUMBER(S) <b>AOARD-094129</b>
12. DISTRIBUTION/AVAILABILITY STATEMENT <b>Approved for public release; distribution unlimited</b>		
13. SUPPLEMENTARY NOTES		

#### 14. ABSTRACT

NLU response at six different locations along the gage length of dog-bone sample is captured with fair degree of accuracy. Nonlinear ultrasonic technique has been used to characterize fatigue damage by Jayrao et.al. (2008), Komareddy et.al. (2006), Cantrell and Yost (2001). The maximum load was 80% of the yield stress with load ratio 0.1.  $A_2/A_{12}$ , ratio of second harmonic amplitude and square of fundamental amplitude, was taken as a measure of nonlinearity parameter. In case of piezoelectric transducer as receiver,  $A_2/A_{12}$  found to increase as the number of fatigue cycle increases up to 47% of fatigue life and it remains constant till 70% of fatigue life. After that it decreases till 93% of fatigue life and it shoots up near the fracture site. Similar results are obtained in low input wave amplitudes. Transmission Electron Microscopy was carried out for samples fatigued for zero%, 47%, and 100% fatigue life. TEM images show that there is increase in dislocation density as the fatigue life of the material increases. Hikata et.al. (1965) reported that nonlinearity parameter ( $A_2/A_{12}$ ) increases as the dislocation density increases. Results showed that there was an increase of around ~250% in the nonlinear parameter  $A_2/A_{12}$  in completely fatigued sample when compared to the as received sample for high input wave amplitudes. It was also observed that for low input wave amplitudes this change was ~450%. Laser vibrometer was also used as receiver to carry out comparative study between contact type and non-contact type receivers. .  $A_2/A_{12}$  showed an increment of 36.2% and 30.3% from the virgin state of the material for samples fatigued up to 47% and 93% of fatigue life respectively in high amplitude regime whereas in the low amplitude regime this percentage increment is 35.7% and 38.3%. Simulations were carried out to examine the applicability region of the solution non-linear wave equation given by Tierston and Thompson (1977) and Cantrell (1984). To simulate the experimental environment one dimensional nonlinear chain embedded in two linear media of same impedance was considered. Simulations were carried out on the chain using FDTD. The second harmonic amplitude was evaluated using pulse inversion technique. Linear relationship of second harmonic amplitude and static displacement with square of input amplitude, nonlinearity parameter, square of wave number and distance of propagation were verified. It was found that solution to nonli-near wave equation given by Tierston and Thompson (1977) and Cantrell (1984) is valid only for small nonlinearities i.e. second harmonic amplitude should be less than five percent of input wave amplitude.

#### 15. SUBJECT TERMS

**nondestructive evaluation, ultrasonics , nonlinear ultrasonics, ultrasonics modeling**

#### 16. SECURITY CLASSIFICATION OF:

a. REPORT

**unclassified**

b. ABSTRACT

**unclassified**

c. THIS PAGE

**unclassified**

#### 17. LIMITATION OF ABSTRACT

**Same as  
Report (SAR)**

#### 18. NUMBER OF PAGES

**88**

#### 19a. NAME OF RESPONSIBLE PERSON

## ABSTRACT

**Key words:** Nonlinear ultrasonic technique, Second harmonic generation, nonlinear wave equation, static displacement

Nonlinear ultrasonic harmonic generation system was used to characterize the damage due to fatigue in commercial purity (99.98%) polycrystalline copper. Dog-bone specimens for fatigue damage studies were fabricated. Through transmission experiments using longitudinal ultrasonic wave were performed to monitor NLU response at six different locations along the gage length of dog-bone sample, to ensure that NLU response close to specimen failure region is captured with fair degree of accuracy. Nonlinear ultrasonic technique has been used to characterize fatigue damage by Jayrao et.al. (2008), Komareddy et.al. (2006), Cantrell and Yost (2001). The maximum load was 80% of the yield stress with load ratio 0.1.  $A_2/A_1^2$ , ratio of second harmonic amplitude and square of fundamental amplitude, was taken as a measure of nonlinearity parameter. In case of piezoelectric transducer as receiver,  $A_2/A_1^2$  found to increase as the no. of fatigue cycle increases up to 47% of fatigue life and it remains constant till 70% of fatigue life. After that it decreases till 93% of fatigue life and it shoots up near the fracture site. Similar results are obtained in low input wave amplitudes. Transmission Electron Microscopy was carried out for samples fatigued for zero%, 47%, and 100% fatigue life. TEM images show that there is increase in dislocation density as the fatigue life of the material increases. Hikata et.al. (1965) reported that nonlinearity parameter ( $A_2/A_1^2$ ) increases as the dislocation density increases. Results showed that there was an increase of around ~250% in the nonlinear parameter  $A_2/A_1^2$  in completely fatigued sample when compared to the as received sample for high input wave amplitudes. It was also observed that for low input wave amplitudes this change was ~450%. Laser vibro-

meter OFV-5000 was also used as receiver to carry out comparative study between contact type and non-contact type receivers.  $A_2/A_1^2$  showed an increment of 36.2% and 30.3% from the virgin state of the material for samples fatigued up to 47% and 93% of fatigue life respectively in high amplitude regime whereas in the low amplitude regime this percentage increment is 35.7% and 38.3%.

Simulations were carried out to examine the applicability region of the solution non-linear wave equation given by Tierston and Thompson (1977) and Cantrell (1984). To simulate the experimental environment one dimensional nonlinear chain embedded in two linear media of same impedance was considered. Simulations were carried out on the chain using FDTD. The second harmonic amplitude was evaluated using pulse inversion technique. Linear relationship of second harmonic amplitude and static displacement with square of input amplitude, nonlinearity parameter, square of wave number and distance of propagation were verified. It was found that solution to nonlinear wave equation given by Tierston and Thompson (1977) and Cantrell (1984) is valid only for small nonlinearities i.e. second harmonic amplitude should be less than five percent of input wave amplitude.

## LIST OF SYMBOLS

$A_1$	Amplitude of fundamental frequency
$A_2$	Amplitude of second harmonic frequency
$A_{dc}$	Static Displacement
$\omega$	Angular frequency
$\beta$	Nonlinearity Parameter
$dt$	Time step size
$h$	Space step size
$z$	Distance of propagation
$\sigma$	Stress
$\varepsilon$	Strain
$\rho$	Density of material
$E$	Elastic modulus
$u_t^i$	Displacement of the particle at the $i^{\text{th}}$ node at time $t$ .

# CONTENTS

LIST OF SYMBOLS .....	iv
LIST OF TABLES .....	vii
LIST OF FIGURES .....	viii
1. INTRODUCTION .....	1
1.1 NONLINEAR ULTRASONIC TECHNIQUE .....	2
1.2 NONLINEARITY PARAMETER.....	3
1.3 PULSE INVERSION TECHNIQUE .....	6
1.4 PROBLEM STATEMENT AND SCOPE .....	7
2. LITERATURE REVIEW .....	8
2.1 SECOND HARMONIC .....	8
2.2 STATIC DISPLACEMENT .....	14
2.3 LOW AMPLITUDES .....	19
2.4 SUMMARY .....	21
3. EXPERIMENTAL INVESTIGATION AND RESULTS.....	23
3.1 SAMPLE PREPARATION .....	23
3.2 EXPERIMENTAL SETUP .....	26
3.3 EXPERIMENTAL PROCEDURE .....	28
3.4 NONLINEARITY PARAMETER FROM 2 <sup>ND</sup> HARMONIC.....	30
3.5 NONLINEARITY PARAMETER AT LOW AMPLITUDES.....	31
3.6 RESULTS .....	32
3.6.1 HIGH AMPLITUDE REGIME .....	33
3.6.2 LOW AMPLITUDE REGIME .....	35
3.7 Transmission Electron Microscopy (TEM) ANALYSIS.....	37
3.8 SUMMARY .....	43
4. EXPERIMENTAL DETAILS (LASER VIBROMETER RECEPTION).....	44
4.1 CALIBERATION OF THE EQUIPMENT .....	44

4.2	EXPERIMENTAL SETUP (LASER VIBROMETER RECEPTION).....	45
4.3	EXPERIMENTAL PROCEDURE .....	46
4.4	NONLINEARITY PARAMETER FROM 2 <sup>ND</sup> HARMONIC.....	48
4.5	$A_2/A_1^2$ AT LOW AMPLITUDES .....	49
4.6	RESULTS .....	50
4.7	COMPARISON with PZT RECEPTION METHOD .....	52
4.8	SUMMARY .....	54
4.9	CONCLUSION .....	54
5.	SIMULATION OF WAVE PROPAGATION IN ONE DIMENSION .....	56
5.1	FINITE DIFFERENCE IN TIME DOMAIN .....	56
5.2	ONE DIMENSIONAL NONLINEAR CHAIN.....	57
5.3	SIMULATION DETAILS .....	58
5.4	PULSE INVERSION .....	61
5.5	BOUNDARY CONDITIONS.....	62
5.6	DEPENDENCE OF 2 <sup>ND</sup> HARMONIC AND STATIC DISPLACEMENT ....	63
5.6.1	SQUARE OF INPUT WAVE AMPLITUDE.....	64
5.6.2	NONLINEARITY PARAMETER $\beta$ .....	64
5.6.3	FREQUENCY OF INPUT WAVE.....	64
5.6.4	DISTANCE OF PROPAGATION.....	64
5.7	VERIFICATION.....	67
5.8	CONCLUSION .....	70
6.	DISCUSSION AND CONCLUSIONS .....	71
6.1	DISCUSSION .....	71
6.2	CONCLUSIONS.....	75
	REFERENCES .....	76

## LIST OF TABLES

Table 1 Chemical Properties of Polycrystalline Copper used in Experiments	23
Table 2 Mechanical and Physical Properties of Copper	24
Table 3 Naming of Samples	26
Table 4 Voltage Corresponding to Power Level of RITEC	27
Table 5 Percentage increase in the maximum value of $A_2/A_1^2$ at different stages of fatigue life for both the sets of the specimens in high amplitude regime	35
Table 6 Percentage change of $A_2/A_1^2$ at different stages of fatigue life in low amplitude regime	37
Table 7 Relationship between the RITEC power setting, the input power level to the transducer and the surface displacement as determined by the laser vibrometer for 9 cycle tone burst	45
Table 8 The percentage increase in the maximum value of $A_2/A_1^2$ at different stages of fatigue life from un-fatigued stage for both amplitude regimes in Laser Vibrometer reception technique	52
Table 9 The ratio of $A_2/A_1^2$ obtained from laser reception to PZT reception in both the amplitude regimes	53
Table 10 Important Parameters used in Simulation	60
Table 11 $A_2$ as Percentage of $A_1$ for different input wave amplitudes and distances of propagation for $f=5\text{MHz}$ $\beta=30$	68
Table 12 $A_2$ as Percentage of $A_1$ for different values of $\beta$ and distances of propagation for $f=5\text{MHz}$ $A_1=4\text{nm}$	69
Table 13 $A_2$ as Percentage of $A_1$ for different values of frequency for $\beta=30$ , $A_1=4\text{nm}$ , $z=6\text{mm}$	69

## LIST OF FIGURES

Figure 1 Amplitude change of Second Harmonic Wave as a function of Fundamental wave Amplitude (a) Aluminum Single Crystal <100> Direction (b) aluminum 2S polycrystal (Hikata <i>et al</i> (1965))	10
Figure 2 Graph of maximum measured value of nonlinearity parameter as function of number of fatigue cycles for aluminum alloy 2024-T4 (Cantrell and Yost (2001))	10
Figure 3 (a) Second Harmonic Amplitude v/s Input Amplitude (b) Pulse Inversion Technique (Kim <i>et al</i> (2006))	11
Figure 4 Graph of calculated material (acoustic) nonlinearity parameter plotted as a function of percent total fatigue life for (a) Polycrystalline Nickel (b) Aluminum alloy 2024-T4	14
Figure 5 Frequency and Fundamental Amplitude Dependence of Static Displacement	15
Figure 6 Acoustic Radiation Induced Static Peak Displacement as a function of Pulse width	15
Figure 7 (a) Amplitudes U of the dc displacement for different HF amplitudes A, measured at the free surface (b) Tone burst $f=22.5$ MHz corresponding to the highest level (Jacob <i>et al</i> (2006))	16
Figure 8 A typical signal output from the experiments on the Al alloy sample showing the automated detection of the maximum and minimum values (Karthik et.al 2007)	17
Figure 9 Displacement profiles generated by a $2\ \mu\text{s}$ toneburst. (a) Displacement pulse obtained for $\beta>0$ . (b) Displacement pulse obtained for $\beta>0$ . (c) Displacement pulse profile obtained oscillatory tail for a dispersive material with $\beta<0$	18
Figure 10 Variation in the static displacement with the distance of propagation for $f=0.796$ MHz, $\nu=30$ , $A=10$ nm, $E=70$ GPa, and density of the material $=2700\ \text{kg/m}^3$ (Karthik <i>et al</i> (2009))	19
Figure 11 Graph of $\beta$ of nontextured polycrystalline Cu–Al alloy plotted as a function of the ultrasonic longitudinal stress wave amplitude. The solid curve is the modeled curve. The filled circles are data obtained from experiments of Bernard for his Cu-Al 8%	20
Figure 12 A typical third harmonic nonlinear response curve plotted as $A_3/A_1^3$ vs. percentage of maximum input power level (Balasubramaniam <i>et al</i> (communicated))	21
Figure 13 Drawing of the Specimen	24
Figure 14 Gauge Length Section	25
Figure 15 100-kN MTS servo hydraulic test system	25
Figure 16 Schematic of Experimental Setup	27
Figure 17 Schematic of through-transmission testing	29
Figure 18 Fixture used to hold sample and transducers	29

Figure 19 Typical Experimentally Received Signal	29
Figure 20 FFT of the Received Signal.	30
Figure 21 Plot of $A_2$ v/s $A_1^2$ for 50,000 cycle fatigued sample for different locations on the sample gauge length	31
Figure 22 The anomalous behavior of $A_2/A_1^2$ as a function of input amplitude for sample is fatigued for 12% of fatigue life.	32
Figure 23 Linear relationship between $A_2$ and $A_1^2$ for as received sample	34
Figure 24 Variation of slope of $A_2$ v/s $A_1^2$ as a function of fraction of fatigue life of the sample in high amplitude regime.	34
Figure 25 The anomalous behavior of $A_2/A_1^2$ in low amplitude regime for un-fatigued sample.	36
Figure 26 The variation of the maximum values of $A_2/A_1^2$ as a function of fraction of fatigue life of the specimen in low amplitude regime	36
Figure 27 Dislocation Pileup near to grain boundary in as received sample	39
Figure 28 Distributed Individual Dislocations in as received sample	39
Figure 29 Tangled Dislocations in the specimen fatigued for 47% of fatigue life	41
Figure 30 Dislocation Bands and Cluster dislocations in the specimen fatigued for 47% of fatigue life	41
Figure 31 Cell Structure with tangled dislocations formed in completely fractured specimen	42
Figure 32 Cell structure in completely fractured specimen surrounded by filler dislocations	42
Figure 33 Experimental setup for Laser Vibrometer Reception Technique	46
Figure 34 Typical Experimentally Received Signal	47
Figure 35 FFT of the Received Signal.	48
Figure 36 Plot of $A_2$ v/s $A_1^2$ as received sample for different locations on the sample gauge length	49
Figure 37 The anomalous behavior of $A_2/A_1^2$ as a function of input amplitude for zero cycle fatigued sample	50
Figure 38 The variation of $A_2/A_1^2$ as a function of fatigue life for LDV reception	51
Figure 39 The variation of the maximum values of $A_2/A_1^2$ as a function of fraction of fatigue life of the material in low amplitude regime	52
Figure 40 The variation of $A_2/A_1^2$ for both types of reception techniques as a function of fraction of fatigue life in high amplitude regime	53
Figure 41 The variation of $A_2/A_1^2$ for both types of reception techniques as a function of fraction of fatigue life in low amplitude regime	54
Figure 42 One Dimensional Chain in FDTD	56

Figure 43 One Dimensional Nonlinear Chain considered for the Simulations	58
Figure 44 The two pulses at the receiver where the blue is in-phase and red is out-of-phase	61
Figure 45 The resultant 2nd harmonic pulse after adding the 2 pulses shown in Figure 3	62
Figure 46 Variation of the Second Harmonic Amplitude and Static Displacement Component with the square of Amplitude of the input wave for different distances of propagation for an input wave of frequency $f = 5\text{MHz}$ , $\beta = 30$	65
Figure 47 Variation of the Second Harmonic Amplitude and Static Displacement Component with the nonlinearity parameter for different distances of propagation for $f=5\text{MHz}$ , $A=4\text{nn}$	66
Figure 48 Variation of the Second Harmonic Amplitude and Static Displacement Component with the square of frequency for $z=6\text{mm}$ , $\beta=30$ , $A=4\text{nn}$	66
Figure 49 Variation of the Second Harmonic Amplitude and Static Displacement Component with Distance of Propagation for different Input wave amplitudes for $f=5\text{MHz}$ , $\beta=30$	67
Figure 50 Variation of slope of $A_2$ v/s $A_1^2$ as a function of fraction of fatigue life of the sample in high amplitude regime	73
Figure 51 The variation of the maximum values of $A_2/A_1^2$ as a function of fraction of fatigue life of the specimen in low amplitude regime	73
Figure 52 Filler dislocations and tangled dislocations in completely fatigued specimen	74
Figure 53 Variation of the longitudinal mode nonlinear parameter with the percentage of fatigue life. (Specimen fatigue loaded at 90% of yield strength).	74

## **1. INTRODUCTION**

ASTM defines the fatigue as the process of progressive localized permanent structural changes occurring in a material subjected to conditions that produce fluctuating stresses at some point or points and that may culminate in cracks or complete fracture after a sufficient number of fluctuations. It has become an important consideration in the design of high performance, safety critical structures and components, as fatigue failure constitutes nearly 70% of failures in dynamically loaded components. The components cannot be designed just based upon the material's yield strength and endurance limit of stress, but must also take into account the defects arising out of material processing, mechanical dynamic loading as well as environmental degradation, which result in reduced strength. Safe-life and damage-tolerant design philosophies of high-performance structures have driven the development of various methods that attempt to evaluate non-destructively the accumulation of damage in such structures resulting from cyclic straining.

One of the powerful nondestructive ways of evaluating material degradation is the ultrasonic method since the characteristics of ultrasonic wave propagation are directly related to the properties of the material. Traditional ultrasonic NDE is based on linear theory and normally relies on measuring some particular parameter (sound velocity, attenuation, transmission and reflection coefficients) of the propagating signal to determine the elastic properties of a material or to detect defects. However, the conventional ultrasonic technique is sensitive to gross defects or opens cracks whereas it is less sensitive to evenly distributed micro-cracks or degradation. An alternative promising technique to overcome this limitation is nonlinear ultrasonics. The principal difference between linear and non-linear ultrasound (NLU) NDE is that in NLU there exist the

higher order harmonic components in the received signal. This is related propagation of finite amplitude (especially high power) ultrasound and its interaction with discontinuities, such as cracks, interfaces and voids. NLU is one among the technique which can be used for the defects of the range from  $1\mu\text{m}$ - $1\text{nm}$ .

In literature NLU is reported as a technique which can be used to characterize the microstructure change caused by cyclic loading of the material. Nonlinear ultrasonics has the potential to quantify distributed damage at the micro-scale, before the formation of macro-cracks, and has a significant potential for the characterization of mechanical and thermal damage such as fatigue, creep, corrosion and over-stress conditions. Most of the research in this area is concentrated on the nonlinearity produced in the materials using the bulk waves (longitudinal). The high amplitude bulk waves get distorted as they pass through the material and gives rise to the generation of higher order harmonic components in the received signal.

## **1.1 NONLINEAR ULTRASONIC TECHNIQUE**

Hooke's Law has been derived on the assumption of infinitesimal amplitude of the ultrasonic or elastic waves propagating in the homogeneous material. However, materials in nature are in general nonlinear, and it is not unusual that the amplitudes of ultrasonic waves used for the inspection are so large that the assumption of infinitesimal disturbance fails. For example when an infinitesimal amplitude elastic wave propagates in copper, Hooke's law is a good approximation because the nonlinear elasticity of a material is insignificant. For finite amplitudes, however the stress-strain relation does not obey the Hooke's law and the nonlinear term in this relation becomes significant.

Nonlinear ultrasonics broadly encapsulates acousto-elastic effect and finite amplitude ultrasonics. The acousto-elastic effect technique requires application of stress and measurement of small changes in the sound velocity in the material. In most cases this technique is not considered to be very practical as very small changes in velocity has to be measured. Hence in the recent times the term nonlinear ultrasonics is used to refer exclusively to finite amplitude ultrasonic technique. In the finite amplitude ultrasonic technique an ultrasonic wave of sufficiently large strain amplitude is introduced in to the material. Due to micro elastic plasticity (nonlinear elasticity) of the material the input wave distorts as it propagates. This is attributed to the difference in the wave velocities of the compression half cycle and the rarefaction half cycle.

In characterizing the materials using nonlinear ultrasonic technique, the Nonlinearity parameter ( $\beta$ ) is a key parameter which represents the nonlinear elastic characteristics of material. It is evaluated using the amplitude of the generated second harmonic. The nonlinearity parameter is an intrinsic property of the material and is very sensitive to inter-atomic changes and the presence of micro level defects in the material.

## 1.2 NONLINEARITY PARAMETER

The nonlinear parameter in terms of the generated second harmonic and the amplitude of the fundamental frequency is derived by Thompson and Tiersten (1977) by solving the nonlinear wave equation using the nonlinear version of Hooke's law. The nonlinear stress strain relationship can be represented as

$$\sigma = E\epsilon(1 - \frac{\beta}{2}\epsilon) \quad (1.2.1)$$

where  $\sigma$ ,  $\epsilon$ , and  $\beta$  are the stress, strain and the nonlinear parameter respectively and  $E$  is the elastic modulus of the material. The equation of longitudinal wave propagating in material can be written as

$$\rho \frac{\partial^2 u}{\partial t^2} = \frac{\partial \sigma}{\partial x} \quad (1.2.2)$$

where  $u$  is the displacement and  $x$  is the direction of propagation of the wave. Using (1.2.1) and (1.2.2) and neglecting the third and higher order terms

$$\rho \frac{\partial^2 u}{\partial t^2} = E \frac{\partial \epsilon}{\partial x} (1 - \beta \epsilon) \quad (1.2.3)$$

The strain  $\epsilon$ , can be written as

$$\epsilon = \frac{\partial u}{\partial x} \quad (1.2.4)$$

Substituting (1.2.4) in (1.2.3) we can obtain the nonlinear wave equation for the displacement  $u(x, t)$  in the solid material, for a plane wave, which is made to pass in to the sample as

$$\rho \frac{\partial^2 u}{\partial t^2} = E \frac{\partial^2 u}{\partial x^2} (1 - \beta \frac{\partial u}{\partial x}) \quad (1.2.5)$$

In order to obtain the solution to nonlinear wave equation represented by (1.2.5) and expression of amplitude of 2<sup>nd</sup> harmonic signal asymptotic procedure is used. In this procedure steady state boundary condition is used, which is

$$u_0 = U_0 \cos(\omega t - kx) \text{ at } x=0. \quad (1.2.6)$$

Solution for the linear wave equation by dropping the nonlinear term can be obtained as

$$u = U_0 \cos(\omega t) \quad (1.2.7)$$

In the second step the solution of homogeneous wave equation (1.2.7) is substituted in the nonlinear part of the nonlinear wave equation (1.2.5) and solution of this resulting equation is assumed to be of the form

$$u_1 = A_0 + A_1 \cos(\omega t - kx) + B_1 \sin(\omega t - kx) + A_2 \cos 2(\omega t - kx) + B_2 \sin 2(\omega t - kx) \quad (1.2.8)$$

After substituting assumed solution in the linear part of the wave equation (1.2.8) coefficients of trigonometric functions are compared. On employing the boundary condition (1.2.6) the expressions of  $A_1$ ,  $B_1$ ,  $A_2$ , and  $B_2$  can be obtained as

$$\begin{aligned} A_1 &= U_0 \\ B_1 &= 0 \\ A_2 &= \frac{1}{8} \beta k^2 A_1^2 z \\ B_2 &= 0 \end{aligned} \quad (1.2.9)$$

The nonlinearity parameter  $\beta$  can be defined as

$$\beta = \frac{8A_2}{zk^2 A_1^2}$$

where  $A_2$ ,  $k$ ,  $z$  and  $A_1$  denote the amplitude of the second harmonic in the received signal, wave number distance of propagation and amplitude of fundamental frequency respectively.

This solution to the nonlinear wave equation is meant only for small nonlinearity as the higher order nonlinear terms have been neglected in the derivation. The applicability of this equation depends upon the frequency of the probes chosen, thickness of the

sample, velocity of wave in material as well as the value of the nonlinearity parameter for the material.

In experimental situations the nonlinearity parameter  $\beta$  is considered to vary with micro level changes in the material which can be due to damage caused by fatiguing of the material and gives a measure of nonlinearity present in the material. Experimentally, the nonlinear acoustic harmonic generation technique involves the introduction of a tone burst of finite amplitude and finite pulse width into the material under study. The fundamental and higher harmonic amplitudes are found by using the Fourier transform of the distorted signal, and finding the dependence of higher harmonics and  $\beta$  on a sample under various experimental conditions.

### 1.3 PULSE INVERSION TECHNIQUE

Let  $u(x, t)$  be the displacement of any point in nonlinear material through which ultrasonic longitudinal wave is passing through. Then from (1.2.8)  $u(x, t)$  can be written as

$$u(x, t) = A_0 + A_1 \cos(\omega t - kx) + A_2 \cos 2(\omega t - kx) \quad (1.3.1)$$

At the same point the signal with phase difference  $\pi$ ,  $u^\pi(x, t)$  can be written as

$$u^\pi(x, t) = A_0 + A_1 \cos(\omega t - kx + \pi) + A_2 \cos 2(\omega t - kx + \pi) \quad (1.3.2)$$

Which upon simplifying

$$u^\pi(x, t) = A_0 - A_1 \cos(\omega t - kx) + A_2 \cos 2(\omega t - kx) \quad (1.3.3)$$

The resulting signal of addition of (1.3.1) and (1.3.2) will be a waveform with DC shift. Its amplitude will be twice of the second harmonic amplitude

$$u(x, t) + u^\pi(x, t) = 2A_0 + 2A_2 \cos 2(\omega t - kx) \quad (1.3.4)$$

This technique is very useful in computing the even harmonic amplitudes of the signal as it avoids the effort to take Fourier transforms and involvement of unnecessary normalization. In the applicability region of the analytical solution of the nonlinear wave equation there will be only  $2^{nd}$  harmonic in time domain signal and the contribution of higher order even harmonics can be neglected.

## 1.4 PROBLEM STATEMENT AND SCOPE

The scope of the present work is to assess the damage in a material using nonlinear ultrasonic technique fatigue and examine the constraint on different parameters for the applicability of the solution of nonlinear wave equation.

Pure polycrystalline copper was chosen as the material for experimental studies in view of understanding the micro-structural changes. Experiments were carried out to introduce fatigue damage under constant amplitude loading. All specimens were examined for the NLU response using bulk longitudinal mode.

Finite Difference in Time Domain is employed to simulate the nonlinear wave equation for a given value of nonlinearity parameter  $\beta$ . The dependence of  $A_2$  on amplitude of input wave  $A_1$ , distance of propagation  $z$  and fundamental frequency of input signal  $f$  was studied. Constraint on the all listed input parameters to produce small nonlinearities was studied to find the range of validity of the model discussed in section 1.2. The amplitude of second harmonic  $A_2$  was computed in time domain itself using the pulse inversion technique.

## 2. LITERATURE REVIEW

This chapter presents the brief literature survey on the evolution nonlinear ultrasonic technique and its application to damage and material characterization. The literature survey is grouped in three categories work done a) the 2<sup>nd</sup> harmonic related NLU experiments and modeling b) DC component based modeling and experiments c) Low amplitude

### 2.1 SECOND HARMONIC

Nonlinear ultrasonic (NLU) theories were developed in 1960's. Hikata *et al* (1965) were one of the first to observe the changes in the attenuation and the nonlinear parameter with the application of stress in plastically deformed aluminum rectangular specimens having dimensions 0.96cmX0.96cmX12.7cm. They conducted experiments on aluminum single crystal 99.99% pure with <100> crystallographic direction as well as on polycrystalline aluminum commercially known as 2S and 11S, and observed an increase in the second harmonic amplitude with the increase in the tensile stress in the material.

Peter *et al* (1985) computed the acoustic nonlinearity parameter for the heat treatable aluminum alloys 6U61-T6, 2024-T4 and 7075-T551. The measurements were made using a 10 MHz longitudinal ultrasonic transducer for transmission and a capacitive transducer for the detection of the second harmonic. The specimens used in the harmonic generation measurements were manufactured in the form of cylinders, 1-1.5 inch diameter, and 1.5 inch in length. The opposite faces of the specimen are polished to be flat and parallel to less than 0.0001 inch.

Yost and Cantrell (1992) did NLU experiments on heat treated artificially aged temper T6 Al 2024-T4. To monitor the changes in the nonlinearity parameter and the hardness during the transformation, eleven sets of samples were fabricated. Each set included two disks one for T4 reference and another for T6 temper, both of nominal radius 15.9 mm and of lengths 6.3 mm and 20 mm, respectively. The surfaces of the thicker disks were lapped and polished to a surface parallelism of better than 15 arc seconds and a flatness of better than 0.6  $\mu\text{m}$ .

Cantrell and Yost (2001) did NLU experiments for assessment of fatigue damage by launching purely sinusoidal ultrasonic bulk waves of frequency 5 MHz into the samples of AA 2024-T4 alloy using a 1.27 cm diameter lithium niobate PZT. Three ASTM standard ‘dogbone’ specimens of AA2024-T4 were fatigued at a rate of 10 Hz under uniaxial, stress-controlled load at 276 MPa and  $R=0$ . Each specimen was fatigued for a different number of cycles: 0k cycles, 3k cycles, 10k cycles, and 100k cycles. Three cylindrical samples each of length 1.9 cm were cut from the 2.53 cm diameter gauge section of each of the four specimens. The signal was received by an air gap capacitance transducer.

Jayarao *et al* (2008) performed NLU experiments to characterize the fatigue damage in aluminum alloy AA7175-T7351 flat hourglass specimens satisfying ASTM E-8 standards. They used 5MHz and 15MHz as transmitter and receiver of the ultrasonic signal in their experiments. He computed 2<sup>nd</sup> harmonic using both through transmission and surface waves.

In all the above references, researchers have used 2<sup>nd</sup> harmonic generation technique to evaluate the nonlinearity parameter given by the derivation shown in previous chapter

in section 1.2 as well as used the model of Hikata *et al* (1965) of string analogy of dislocations to predict the nonlinearity parameter. Cantrell and Yost (2001) showed in their experimental analysis on fatigue of aluminum alloy AA 2024-T4 that optical microscopical examination of the end surfaces of the samples revealed no cracks longer than 35–40  $\mu\text{m}$  which do not contribute to nonlinearity.

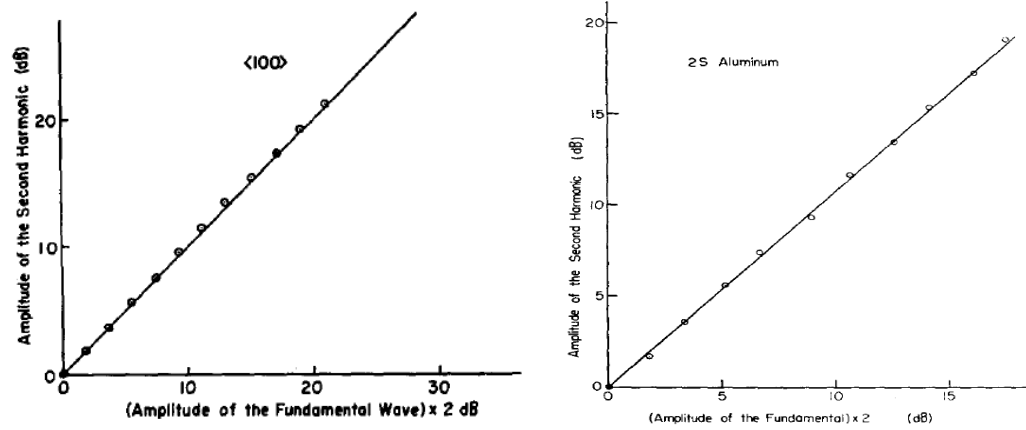


Figure 1 Amplitude change of Second Harmonic Wave as a function of Fundamental wave Amplitude (a) Aluminum Single Crystal  $\langle 100 \rangle$  Direction (b) aluminum 2S polycrystal (Hikata *et al* (1965))

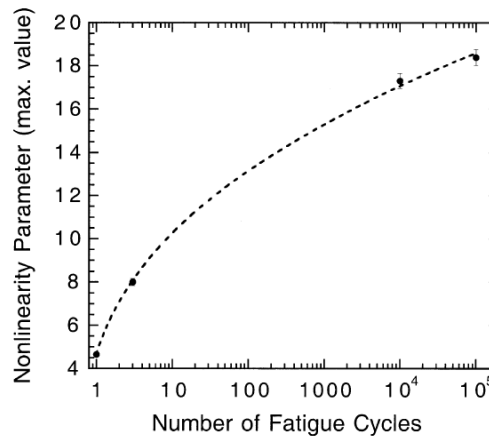
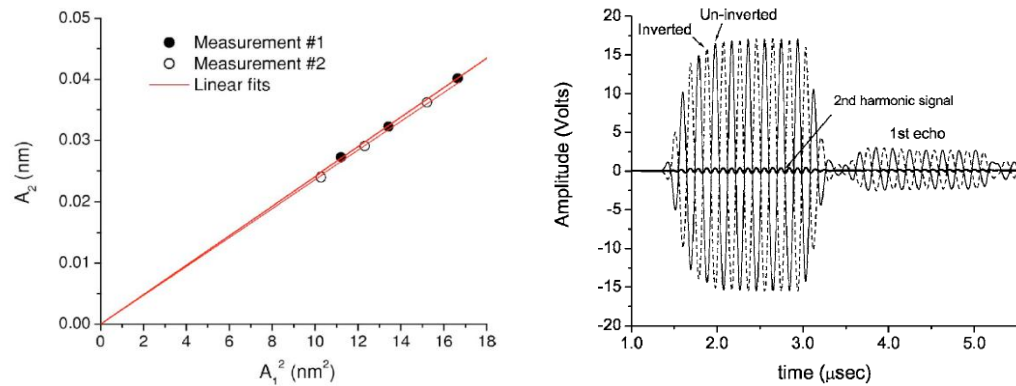


Figure 2 Graph of maximum measured value of nonlinearity parameter as function of number of fatigue cycles for aluminum alloy 2024-T4 (Cantrell and Yost (2001))

Kommareddy *et al* (2006) performed experiments on characterization of fatigue damage of 100% fatigued specimens of Ti 17 and showed an increase of more than 80

percent in nonlinearity parameter from grip region to fracture. They used 5MHz and 10 MHz PZT as transmitter and receiver for experimental analysis and computed the 2<sup>nd</sup> harmonic by taking Fourier transform of received signal. Peter *et al* (1985)'s NLU experiments indicated linear relationship between the nonlinearity parameter and the volume fraction of second phase precipitates in the alloys. Independent measurements made of the acousto-elastic constants in the same alloys are found to exhibit a similar dependence on second phase precipitates. Jayarao *et al* (2008) showed two peak behavior of nonlinearity parameter as a function of fatigue life of aluminum alloy AA7175-T7351. The first peak was reported to happen due to formation of PSBs whereas the second peak due to interaction of PSBs and cracks with cell structures.

Coming on to other techniques to compute second harmonic and nonlinearity parameter, Kim *et al* (2006) reported experimental characterization of fatigue damage in a nickel-base super alloy using nonlinear ultrasonic waves. Signal of 7-9 cycles of 5MHz central frequency is fed to the specimen and received by 10 MHz PZT. The second harmonic is extracted by pulse inversion technique differently from taking the Fourier transform of the received signal.



**Figure 3 (a) Second Harmonic Amplitude v/s Input Amplitude (b) Pulse Inversion Technique (Kim *et al* (2006))**

The nonlinearity parameter is found to increase up to twice of the virgin state as shown in Figure 3(a). They also reported that increment in nonlinearity parameter  $\beta$  in high cycle fatigue is less as compared to low cycle fatigue because defects are localized in high cycle fatigued material whereas in low cycle fatigued material defects are well distributed.

Researchers have also shown possibility to use Rayleigh and Lamb waves for nonlinearity parameter estimation instead of longitudinal waves. Herrmann *et al* (2006) used Rayleigh waves generated from 5 MHz PZT for NLU experiments on Nickel based super-alloy. A signal of 25 cycles was fed to the specimen and with the help of hanning window which was used to take only the steady state part of the received signal. A heterodyne laser interferometer was used as a high-fidelity, point-like detection system. The nonlinearity parameter for their experiments is

$$\beta = \frac{8i\bar{u}_z(2\omega)}{k_l^2 x \bar{u}_z^2(\omega)} \frac{p}{k_R} \left( 1 - \frac{2k_R^2}{k_R^2 + s^2} \right).$$

where  $p^2 = k_R^2 - k_l^2$ ;  $s^2 = k_R^2 - k_s^2$  and  $k_R$ ,  $k_l$ , and  $k_s$  are the wave-numbers for Rayleigh, longitudinal, and shear waves. The fractional nonlinearity parameter is reported to increase monotonically up to three.

Pruell *et al* (2007) and Bermes *et al* (2007) used Lamb waves generated from 25 cycle tone burst of 2.225MHz central frequency for their Experiments on NLU. Both the groups used heterodyne laser interferometer as their receiver.

Researchers also tried modeling the high input amplitude based nonlinearity of the material using string analogy of dislocations. Hikata and Elbaum (1966) were one of the first to derive the expressions of amplitudes of second and third harmonic of the funda-

mental wave. Amplitudes were evaluated using the vibrating string analogy of dislocations and found out the contributions of the factors which are seems to be responsible. Their model predicted that contribution to second harmonic amplitude were two factors a) lattice anharmonicity b) Nonlinear dislocation motion. They also reported that the third harmonic amplitude does not depend upon lattice anharmonicity at room temperature where the dependence thermal expansion coefficient is small. The amplitudes of second and third harmonics are proportional to square and cube of the amplitude of fundamental wave as long as the dislocation loop lengths remain same. Hikata *et al* (1965) modeled the interaction of an ultrasonic wave with dislocation using vibrating string analogy of dislocations. Their model predicted the variation of the nonlinearity parameter directly with the dislocation density and the fourth power of the dislocation loop length. This increase in loop length was attributed to the dislocation displacement due to the applied stress.

Cantrell (2006) derived the expressions for contribution to nonlinearity parameter from monopole and dipole dislocations and cracks using the string analogy model of Hikata *et al* (1965). He found that nonlinearity parameter for monopole dislocations is directly proportional to dislocation density and fourth power of dislocation loop length whereas it is inversely proportional to square of Berger's vector. Similarly, contribution to nonlinearity parameter from dipole dislocations is proportional to dislocation density and cube of distance between opposite poles whereas inversely proportional to Berger's vector. Through this model, he was able to predict the nonlinearity parameter for polycrystalline Nickel and validated from the experiments.

$$\beta^{\text{mp}} = \frac{24 \Omega \Lambda^{\text{mp}} L^4 R^3 (A_2^e)^2}{5 G^3 b^2} |\sigma_0|. \quad \beta^{\text{dp}} = \frac{16 \pi^2 \Omega R^2 \Lambda^{\text{dp}} h^3 (1 - \nu)^2 (A_2^e)^2}{G^2 b}.$$

$$\beta = \frac{\beta^e + \beta^{\text{mp}} + \beta^{\text{dp}}}{(1 + \Gamma^{\text{mp}} + \Gamma^{\text{dp}})^2} \quad \Gamma^{\text{mp}} = \frac{2}{3} \left( \frac{\Omega \Lambda^{\text{mp}} L^2 R}{G} \right) A_2^e \quad \Gamma^{\text{dp}} = \frac{4 \pi A_2^e \Omega R \Lambda^{\text{dp}} h^2 (1 - \nu)}{G}.$$

The figure below shows the calculated material (acoustic) nonlinearity parameter from the above expressions which are validated by experiments.

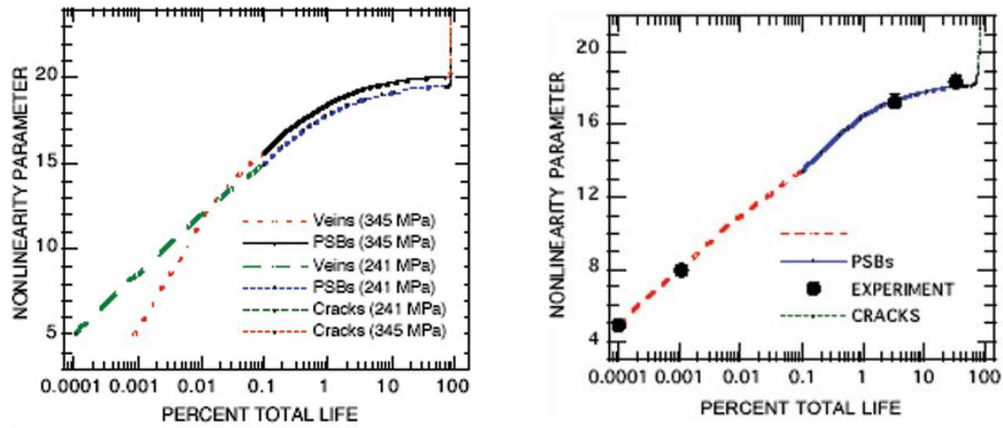
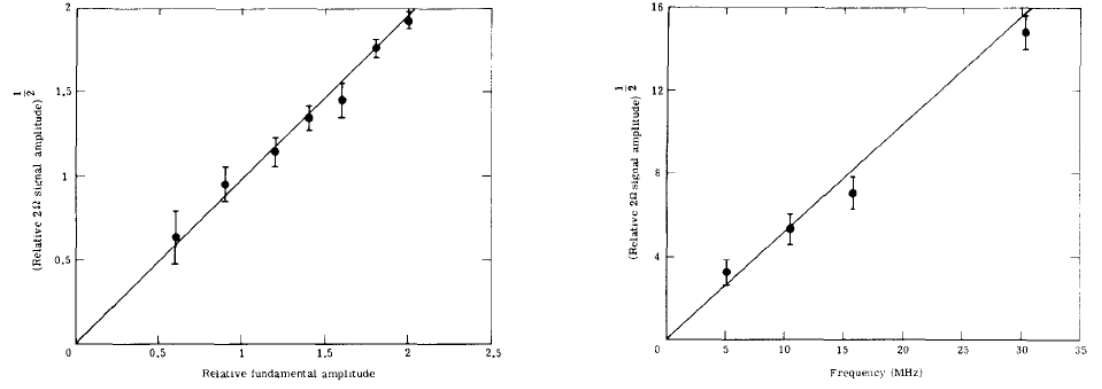


Figure 4 Graph of calculated material (acoustic) nonlinearity parameter plotted as a function of percent total fatigue life for (a) Polycrystalline Nickel (b) Aluminum alloy 2024-T4

## 2.2 STATIC DISPLACEMENT

Cantrell and Winfree (1984) were one of those who showed experimental evidence of DC component through their experiments on single crystal Germanium [111]. If the drive amplitude variation is made to occur sinusoidally at a lower frequency  $\omega$  than frequency  $f$ , then the dc component will be observed at  $2\omega$ . Further, the amplitude at  $2\omega$  would have the same drive amplitude and frequency dependencies as the un-modulated static displacement term.



**Figure 5 Frequency and Fundamental Amplitude Dependence of Static Displacement**

Yost and Cantrell (1984) did their experiments on single crystal silicon along [110] direction and vitreous silica to generate static displacement pulses having shape of right angled triangle. They found that the nonlinearity parameter was positive for silicon and negative for vitreous silica. Calculation of nonlinearity parameter is done from the absolute measurement of slope of static displacement pulse and the amplitude of ultrasonic toneburst.

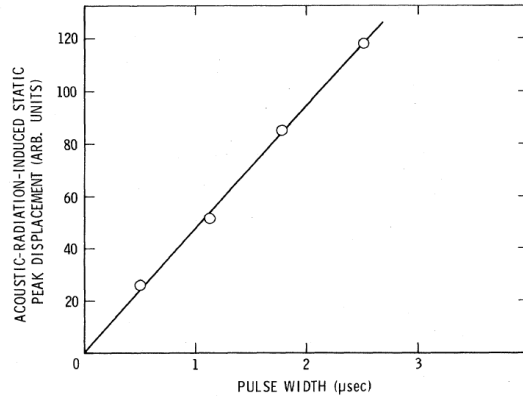


**Figure 6 Acoustic Radiation Induced Static Peak Displacement as a function of Pulse width**

Jacob *et al* (2006) studied measurements of the static displacement induced by the radiation stress associated with a longitudinal acoustic wave propagating in a solid. Long acoustic tone bursts cycle number larger than 20, with a carrier frequency  $f$  close to 20

MHz, were launched by piezoelectric transducers into fused silica  $\beta$  (silica=−7.4) and duraluminum  $\beta$  (dural=11.8) samples. The static displacement was measured at the sample free surface with an optical interferometer. Static displacement pulses were found to have a shape of rectangular topped pulse in contrary to Yost and Cantrell (1984) right-triangular shaped static displacement pulses. They pointed out that in Yost and Cantrell experiments, the capacitive detector and the lithium niobate transducers cover the whole surface of the samples, whereas in their configuration the piezoelectric transducers are much smaller than the sample cross section, and the lateral resolution of the laser is less than 50 m. So the effect of the spatial distribution of the acoustic energy could be implied in the shape of the dc pulse. In their conclusion, they mentioned that diffraction and attenuation effects must be taken into account to complete their physical description of the phenomenon.

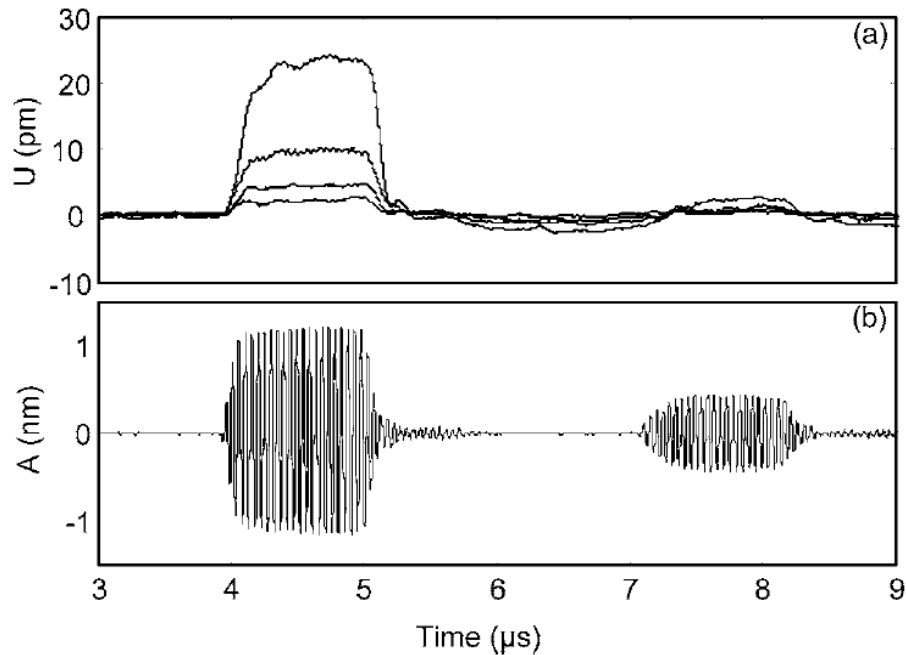


**Figure 7 (a) Amplitudes  $U$  of the dc displacement for different HF amplitudes  $A$ , measured at the free surface (b) Tone burst  $f = 22.5$  MHz corresponding to the highest level (Jacob *et al* (2006))**

Karthik *et al* (2007) gave a simplified technique to compute dc component in time domain itself. According to this technique dc component is half of the difference of the absolute values of average values of peaks and troughs of time domain signal.  $dc = (abs(A)-abs(B))/2$  where A and B are average values of peaks and troughs of time domain signal. The experiments on AA7175-T7351 were validated by modeling in which static strain induced displacement is found to be independent of width of tone burst signal. The shape of the pulse was reported to be of rectangular shape which was in accordance with Jacob *et al* (2006).

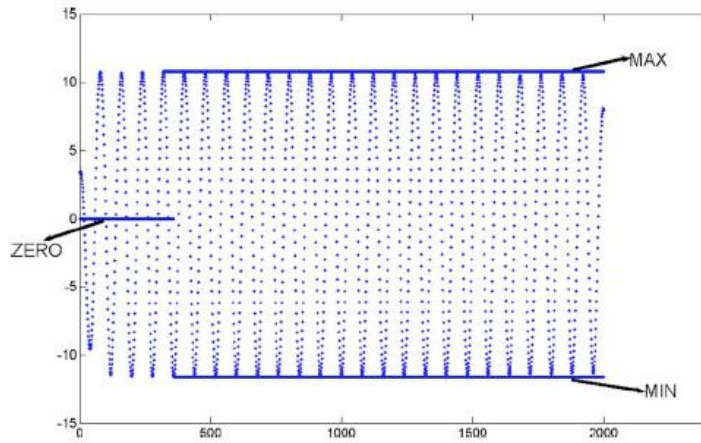


**Figure 8 A typical signal output from the experiments on the Al alloy sample showing the automated detection of the maximum and minimum values (Karthik et.al 2007)**

Cantrell (2008) derived expressions for static displacement by taking into account the dispersion and attenuation. According to this publication the propagating wave experiences a larger attenuation in polycrystalline metals than in mono-crystals given by  $\exp(-a_0 z f^2)$  where  $f$  is the frequency and  $a_0$  is the attenuation coefficient. It is shown that the shapes of acoustic radiation-induced static strain and displacement pulses are defined locally by the energy density of the generating waveform. The diffraction and attenuation produce dramatic changes in the shape of static displacement pulses when using

laser detection. The effects of dispersion on static pulses are obtained by including a dispersive term in the phase of the particle velocity solution to the nonlinear wave equation. The dispersion causes an evolutionary change in the shape of the energy density profile that leads to the generation of solitons experimentally observed in fused silica. According to him Piezoelectric transducers are sensitive not to displacements but rather to strains. Thus, the pulse profiles Karthik *et al* (2007) reported are not displacement profiles. They are strain profiles and their results are in agreement with the predictions of the present model for strain pulses.

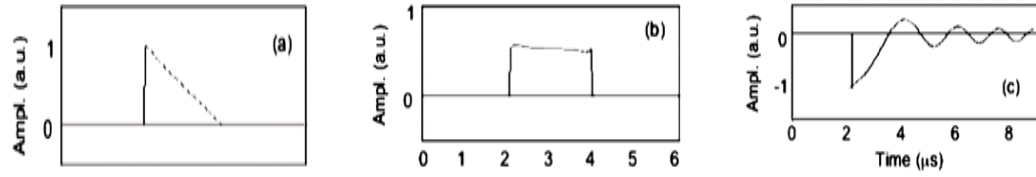


**Figure 9 Displacement profiles generated by a 2  $\mu$ s toneburst. (a) Displacement pulse obtained for  $\beta > 0$ . (b) Displacement pulse obtained for  $\beta > 0$ . (c) Displacement pulse profile obtained oscillatory tail for a dispersive material with  $\beta < 0$**

Karthik *et al* (2009) modeled the nonlinear wave equation by FDTD and showed that the shape of the static displacement pulse is rectangular in shape rather than right triangle topped. Another finding was that the DC component value does not depend upon the pulse width of the input signal rather it is directly the distance of propagation. They argued that pulses reported by Cantrell (2008) are because of the capacitive detection system.

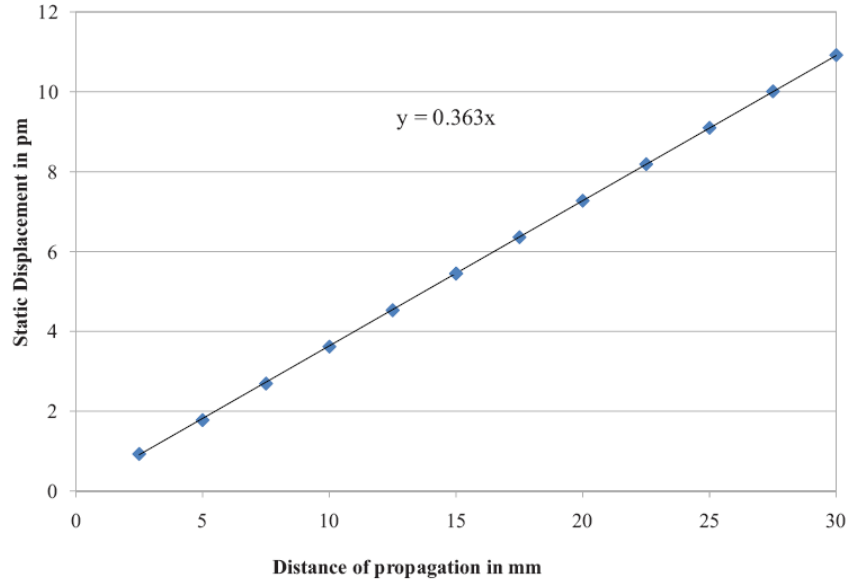


**Figure 10** Variation in the static displacement with the distance of propagation for  $f=0.796$  MHz,  $\lambda=30$ ,  $A=10$  nm,  $E=70$  GPa, and density of the material  $=2700$  kg/m<sup>3</sup> (Krthik *et al* (2009))

## 2.3 LOW AMPLITUDES

Cantrell (2009) derived an analytical model of the effects of the Peierls–Nabarro barrier stress due to lattice planes on the nonlinear dynamics of dislocation motion in crystalline solids resulting from a perturbative ultrasonic wave. From his model, he found the nonlinearity parameter to be functionally dependent on the magnitude of the Peierls–Nabarro barrier stress, the dislocation loop length, the shear modulus, and the Burgers vector of the crystal. A sharp increase in the magnitude of  $\beta$  is shown to occur at low ultrasonic amplitudes where the dislocation motion is confined between adjacent lattice planes (quiescent lattice planes) bounding the unperturbed dislocation in rest position. Under such circumstances the pinning forces become relatively less important to the dislocation motion and the entire dislocation moves relatively unimpeded in the region between the quiescent lattice planes. The result is a large increase in the loop

length. The increase in the loop length leads to a dramatic increase in  $\beta$  over the range of amplitude corresponding to dislocation motion within the quiescent lattice planes. For poly-crystals the sessile grain boundary dislocations may also make a substantial contribution to the low amplitude enhancement. Experimental observations of the hook-like shape known as the Buck hook have been reported in Bernard et.al. but the phenomenon has been previously unexplained. The present model shows that the Buck hook is a consequence of dislocation dynamics at low ultrasonic drive amplitudes.

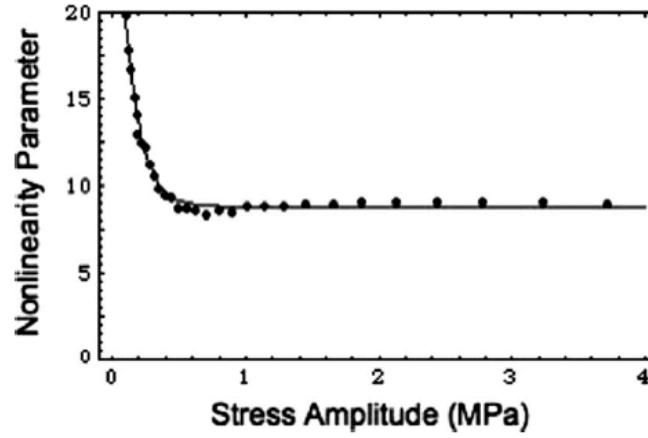


**Figure 11 Graph of  $\beta$  of nontextured polycrystalline Cu–Al alloy plotted as a function of the ultrasonic longitudinal stress wave amplitude. The solid curve is the modeled curve. The filled circles are data obtained from experiments of Bernard for his Cu–Al 8%**

Balasubramaniam *et al* (communicated) reported that if ratio of third harmonic and cube of the fundamental amplitude in Fourier transform is plotted against the input amplitude then the curve fitting relationship is given by

$$\left( \frac{A_3}{A_1^3} \right) = a e^{-b A_0}$$

where  $a$  and  $b$  are adjustable fitting parameters. They plotted the void density content (total void area divided by the total area in the microphotograph), expressed as a

percentage, as a function of the fitting constants  $a$  and  $b$ . They found the following relationships: (a) a logarithmic relationship exists between the fitting parameter, ' $a$ ', and the percentage void content, and (b) a linear relationship exists between the parameter, ' $b$ ', and the percentage void content. The constant ' $a$ ' that accounts for the increase in the loop length and the factor ' $b$ ' govern the rate at which the transition occurs.

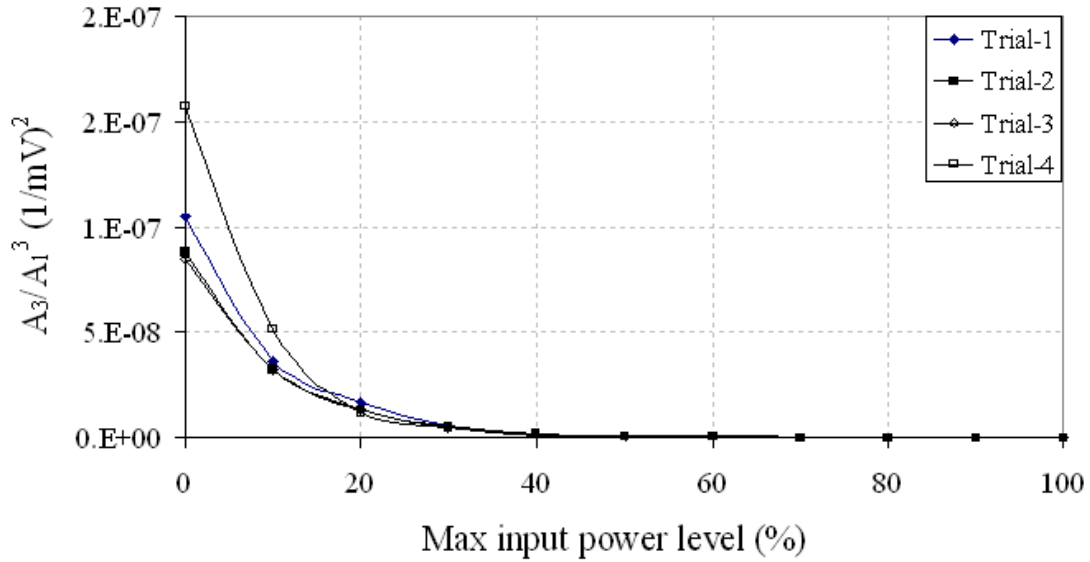


Figure 12 A typical third harmonic nonlinear response curve plotted as  $A_3/A_1^3$  vs. percentage of maximum input power level (Balasubramaniam *et al* (communicated))

## 2.4 SUMMARY

Second harmonic generation technique has been used for material characterization and fatigue characterization at different stress levels in plastic region. Researchers like Cantrell (1984) and Hikata *et al* (1965) have related the increase in nonlinearity parameter to metallographic studies at high input amplitudes. At the same time anomalous behavior of nonlinearity parameter has been explained recently by Cantrell (2009). The

high nonlinearity parameter value at very low input amplitudes have been utilized to characterize the creep damage by Jitendra (2009) but has not been used to characterize the fatigue damage. Traditional longitudinal ultrasonic transducers are used by many researchers whereas capacitance based receiver is been used by Cantrell group. Coming to the solution of nonlinear wave equation which is solved only for small nonlinearities by neglecting the higher order terms by Tierston and Thompson (1977) is been referred in approximately every citation related to NLU but very less researchers have mentioned the range of nonlinearity in which they worked in. Constraints on input parameters have not been studied yet by simulations. Karthik *et al* (2009) has modeled the equation by using FDTD but did not talk about the range in which the solution to it is applicable. This literature survey gave us the base to define the problem statement and plan of the work.

### 3. EXPERIMENTAL INVESTIGATION AND RESULTS

This chapter deals with NLU experiments which were carried out to characterize the damage due to fatigue. To simulate these damages, pure polycrystalline copper specimens were fabricated and tested on a computer controlled test system. Details of the sample preparation for experiments are presented in Section 3.1. Experimental setup is presented in Section 3.2. Experimental procedure for nonlinear ultrasonic measurements using the RITEC RAM-5000 system for this technique is described in the subsequent Section 3.3.

#### 3.1 SAMPLE PREPARATION

Dog-bone specimens were fabricated from 8 mm thick rolled strips of pure polycrystalline copper, conforming to ASTM E-08 standards, for fatigue damage studies. Table 1 and Table 2 represent the chemical and mechanical properties of the polycrystalline copper respectively.

**Table 1 Chemical Properties of Polycrystalline Copper used in Experiments**

Element	Sn	P	Fe	Bi	S	Cu
Wt %	0.005	0.002	0.004	0.003	0.003	Balance (99.98)

**Table 2 Mechanical and Physical Properties of Copper**

Property	Value
Density	8920 kg/m <sup>3</sup>
Modulus of Elasticity	100 GPa
Melting Temperature	1356 K
Re-crystallization Temperature	394 K
Boiling Temperature	2868 K

Dog-bone specimens as shown in Figure 13 having a nominal thickness of 6 mm and a gage section length of 30 mm were fabricated for fatigue studies. Dog-bone specimen is chosen to localize the cracking behavior in the specimen at one point. The specimen surface was mirror finished. Fatigue loading under constant amplitude loading was performed using a 100-kN MTS servo hydraulic test system (Figure 15).

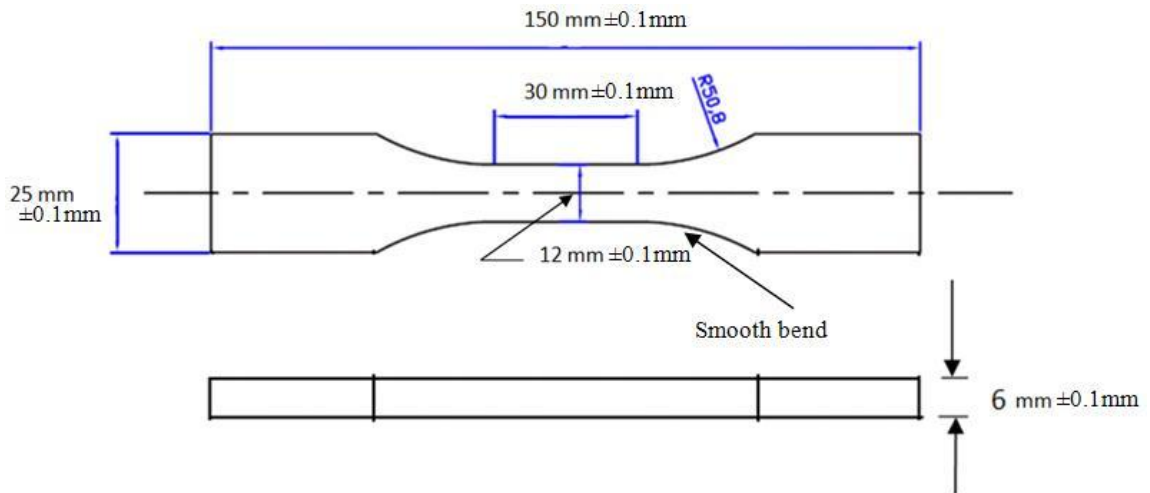


**Figure 13 Drawing of the Specimen**

### Gauge length

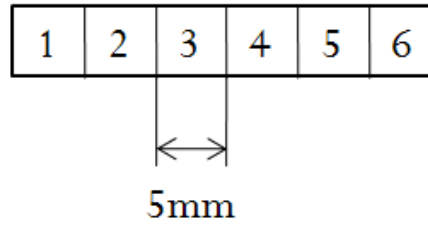


**Figure 14 Gauge Length Section**



**Figure 15 100-kN MTS servo hydraulic test system**

Totally sixteen specimens were prepared: fourteen out of those specimens were tested between a maximum load of 14.62 kN and a minimum load of 1.46 kN (which corresponds ~80% and ~8% of material yield strength), under tension-tension cycling at a test frequency of 20 Hz. Details of cyclic loading of the samples is given in Table 3.

**Table 3 Naming of Samples**

<b>S. No.</b>	<b>Sample Names</b>	<b>No. of Fatigue Cycles</b>
<b>1.</b>	$0_1$ and $0_2$	Zero
<b>2.</b>	$500_1$ and $500_2$	50,000
<b>3.</b>	$1000_1$ and $1000_2$	100,000
<b>4.</b>	$1500_1$ and $1500_2$	150,000
<b>5.</b>	$2000_1$ and $2000_2$	200,000
<b>6.</b>	$3000_1$ and $3000_2$	300,000
<b>7.</b>	$4000_1$ and $4000_2$	400,000
<b>8.</b>	$F_1$ and $F_2$	Till Fracture (4.5 Lac and 4.1 Lac)

All the samples listed in Table 3 have been fatigued for different number of fatigue cycles which are listed in front of their names. The samples having same name but subscripts as 1 and 2 are similar means do not have any difference in experimental procedure and technique. Total fatigue life of the material was taken as average of life of  $F_1$  and  $F_2$  samples.

### **3.2 EXPERIMENTAL SETUP**

For driving the transducer a computer controlled transmitter (RITEC Advanced Measurement system RAM-5000, RITEC) was used that can generate sine waves with an adjustable number of cycles at a single frequency. The RITEC gated RF amplifier module is designed to derive the very high power RF bursts needed for modern transducers. The signal was fed to the material by a PZT of central frequency 5MHz and the output was received by another PZT of 10MHz central frequency. The output from the 10 MHz PZT was fed to Agilent 6032A digital Storage oscilloscope, which operates at a

sampling rate of 100 MHz, for visual inspection as well as for storing the data in CSV format. For further analysis of the data, the digitized data from the oscilloscope was transferred to a USB drive with 1000 data points per window. The experimental set up is as shown in the Figure 16.

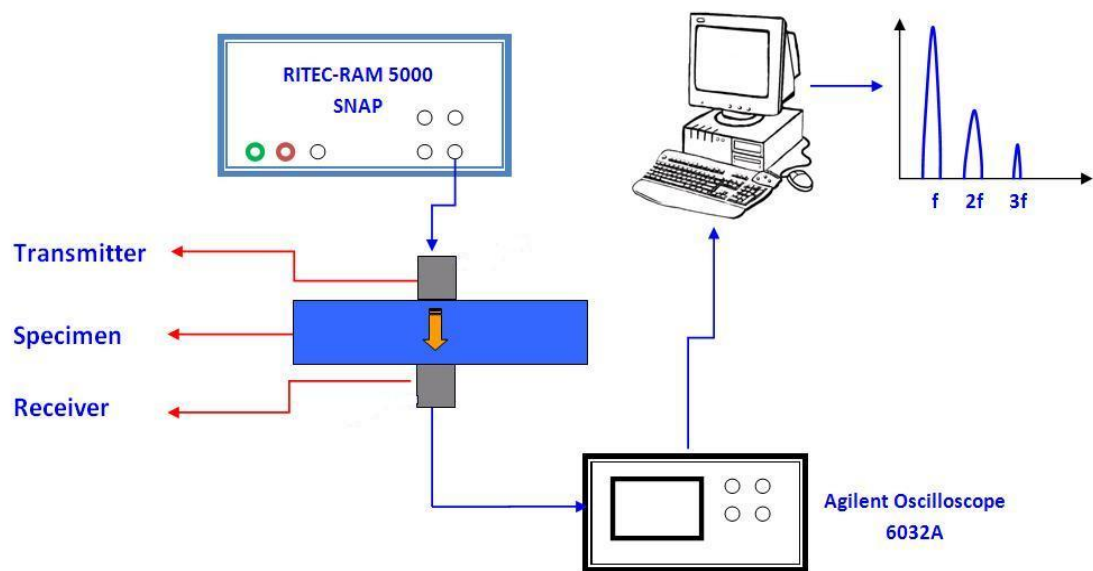


Figure 16 Schematic of Experimental Setup

Table 4 Voltage Corresponding to Power Level of RITEC

RITEC Power Setting	Input Voltage to the Transducer (V)	RITEC Power Setting	Input Voltage to the Transducer (V)
0	68.4	60	990
10	170.5	70	1164
20	322.1	80	1378
30	484	90	1625
40	646	100	1880
50	822		

### **3.3 EXPERIMENTAL PROCEDURE**

The NLU experiment is a through transmission experiment, as shown in Figure 17, in which two ultrasonic transducers are placed on either side of the specimen to transmit and receive the signal. Ultrasonic transducer of diameter of 8.8 mm supplied by PANAMETRIC INC and central frequency 5 MHz was utilized as transmitter and 10 MHz ultrasonic transducer of same dimension and supplier as receiver. In order to get a High power RF tone burst, a RITEC RAM-5000 gated amplifier is used and the output from the receiver is fed to an Agilent 6032A digital Storage oscilloscope, which is operating at a sampling rate of 100 MHz, for visual inspection and as well as for storing the data in CSV format. For further analysis of the data, the digitized data from the oscilloscope is transferred to a USB drive with 1000 data points per window. 50-Ohm cables were used for interconnecting different instruments that are used to minimize the losses. The experimental arrangement is shown in Figure 17 and the fixture used for holding the transducers and the specimen is as shown in the Figure 18. A typical longitudinal mode signal for sinusoidal input pulse and its Fourier transform is shown in Figure 19 and Figure 20.

To capture the signals at different locations on the gauge length, as shown in Figure 14, the specimen is moved so that the particular location is exactly in between the transducers. Coconut oil was used as the couplant between the transducer and sample.

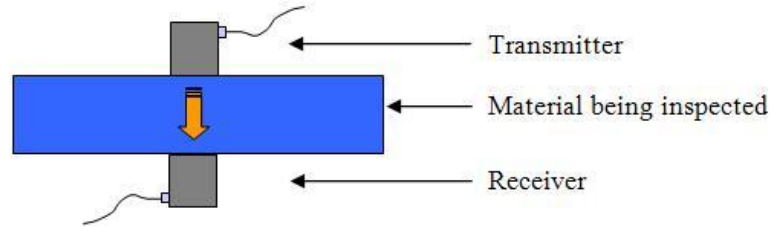


**Figure 17 Schematic of through-transmission testing**

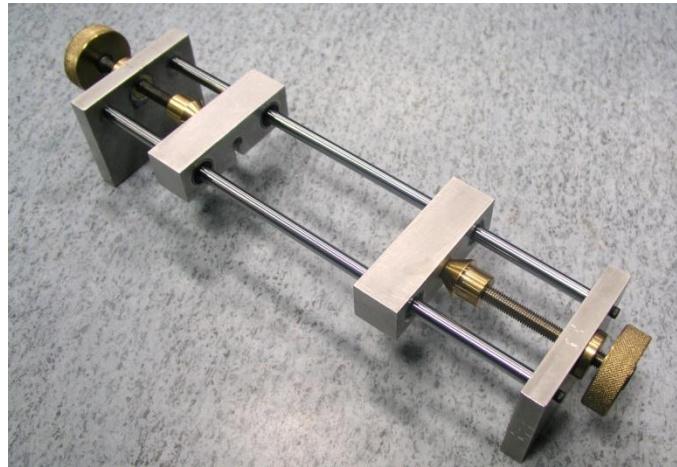


**Figure 18 Fixture used to hold sample and transducers**

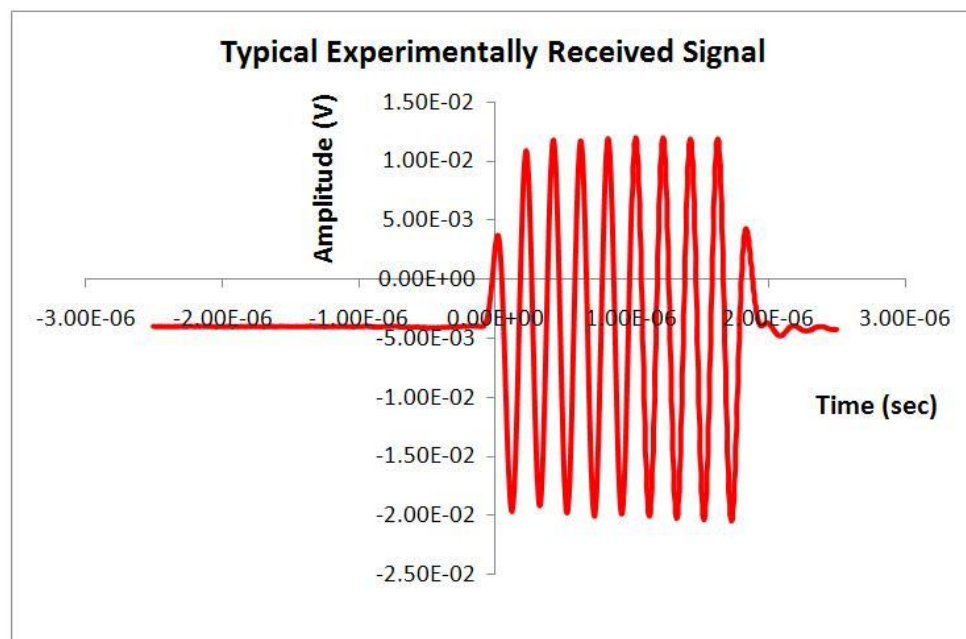


**Figure 19 Typical Experimentally Received Signal**

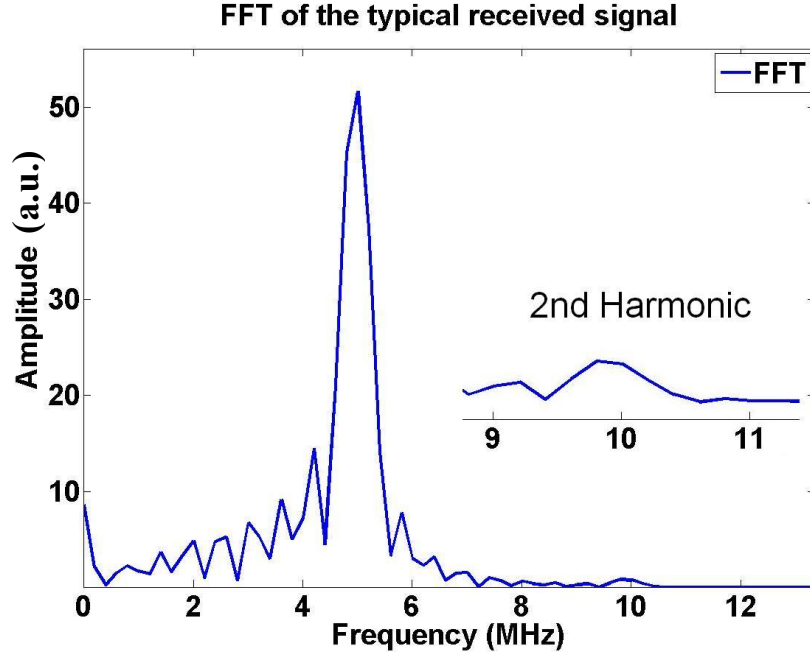


Figure 20 FFT of the Received Signal.

### 3.4 NONLINEARITY PARAMETER FROM 2<sup>ND</sup> HARMONIC

The nonlinearity parameter is defined as

$$\beta = \frac{8A_2}{zk^2A_1^2}$$

or

$$A_2 = \frac{1}{8}\beta k^2 A_1^2 z$$



$$A_2 \propto A_1^2 \text{ for a constant } \beta$$

The expression for second harmonic amplitude indicates that for a constant  $\beta$  the second harmonic amplitude is proportional to square of the fundamental frequency amplitude. Values of  $A_2$  and  $A_1$  are measured in volts so the nonlinearity parameter is expressed as  $A_2/A_1^2$  (slope of  $A_2$  v/s  $A_1^2$  curve). Figure 21 shows the plot of  $A_2$  v/s  $A_1^2$  for

50,000 cycle fatigued sample for different locations on the sample gauge length as shown in Figure 21.

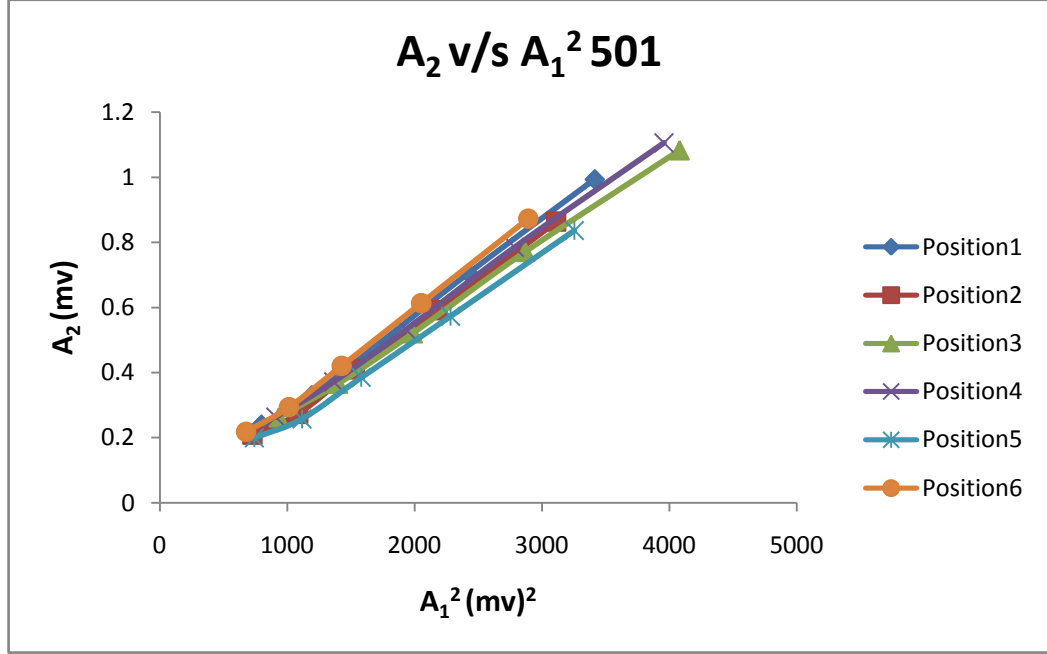


**Figure 21 Plot of  $A_2$  v/s  $A_1^2$  for 50,000 cycle fatigued sample for different locations on the sample gauge length**

The slope of the lines  $A_2 \text{ v/s } A_1^2$  is measured at six different positions on the gauge length. The measurement of  $A_1$  and  $A_2$  are done five times and their average values have been taken for further analysis.

### 3.5 NONLINEARITY PARAMETER AT LOW AMPLITUDES

As described by Cantrell (2009), there exists anomalous behavior of nonlinearity parameter at low input amplitudes. The nonlinearity parameter shows a very high value as compared to the high amplitude regime due to increase in dislocation loop length at this stage. In this experimental study, it was found that the quantity  $A_2/A_1^2$  obtains a very

high value at low input amplitudes as compared to high input amplitudes. Figure 22 shows the anomalous behavior of  $A_2/A_1^2$  as a function of input amplitude for sample which is fatigued for 50,000 cycles. Such plots are plotted for all the samples described in Table 3.

The value of  $A_2/A_1^2$  at lowest possible input amplitude has been considered another representative of nonlinearity parameter.

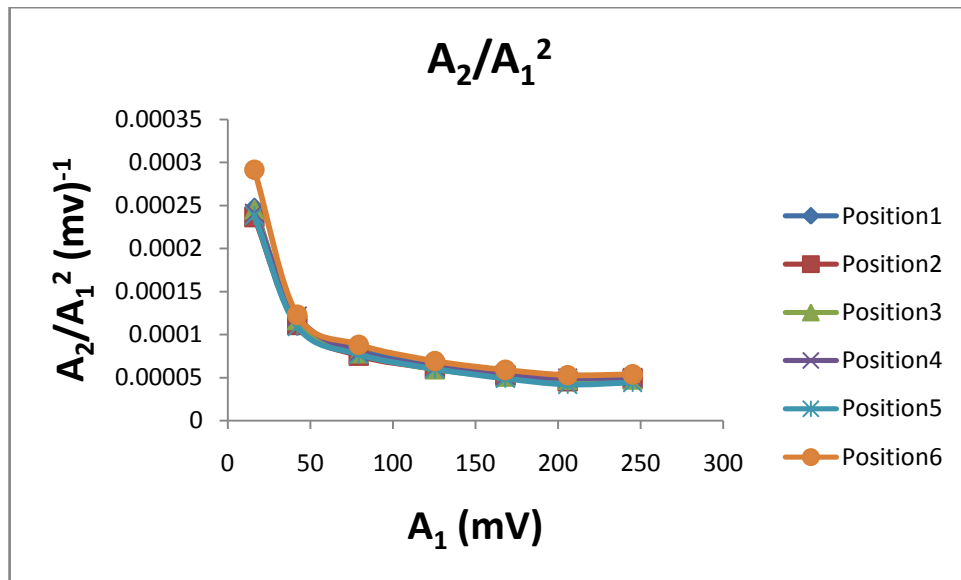


**Figure 22 The anomalous behavior of  $A_2/A_1^2$  as a function of input amplitude for sample is fatigued for 12% of fatigue life.**

### 3.6 RESULTS

For PZT as receiving transducer the experiment were carried out in two regimes of amplitude 1) High Amplitude Regime which is more than 20 percent of maximum input power level 2) Low Amplitude regime which is less than 20 percent of maximum input power level.

### 3.6.1 HIGH AMPLITUDE REGIME

Total 16 specimens were fabricated out of them two were kept unfatigued whereas others were fatigued up to 50k cycles, 100k cycles, 150k cycles, 200k cycles, 300k cycles, 400k cycles and up to fracture. For each stage of fatigue life two samples were fatigued. Later on two different sets have been made randomly having one sample each for every stage of fatigue life of the material. For repeatability of the experiment, the measurement was done five times at each of six different locations on each sample and the values are averaged for every location individually. The variation was found within  $\pm 5\%$ . Different value of  $A_1$  were obtained by changing the power level of RITEC RAM 5000 and corresponding  $A_2$  was obtained by taking the Fast Fourier Transform of the received signal. Figure 23 shows the linear relationship between  $A_2$  and  $A_1^2$  for as received sample which shows the correctness of the readings obtained in the experiment. Similar plots have been plotted for all the specimens. The slope of the straight lines is taken as a measure of the nonlinearity parameter.

Figure 24 shows the variation of the maximum values of  $A_2/A_1^2$  on all the samples along the gauge length in high amplitude regime. The error bars represents the variation across the gauge length of the specimen. The  $A_2/A_1^2$  is found to increase up to 47% of fatigue life then it remains constant till 70% of fatigue life and then decreases at 93% of fatigue life. In the end at the fracture the  $A_2/A_1^2$  is found to have sharp increase in its value.

Table 5 shows the percentage increase in the maximum value of  $A_2/A_1^2$  at different stages of fatigue life from as received stage for both the sets of the specimens in high amplitude regime. The increment at the fractured specimen is found to be more than 200 percent.

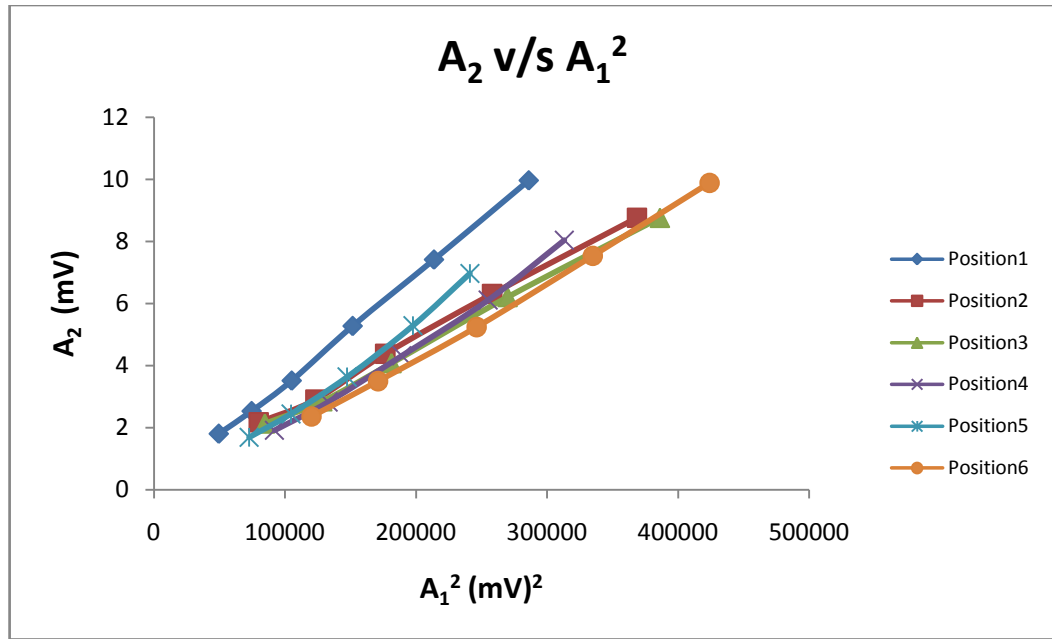


Figure 23 Linear relationship between  $A_2$  and  $A_1^2$  for as received sample

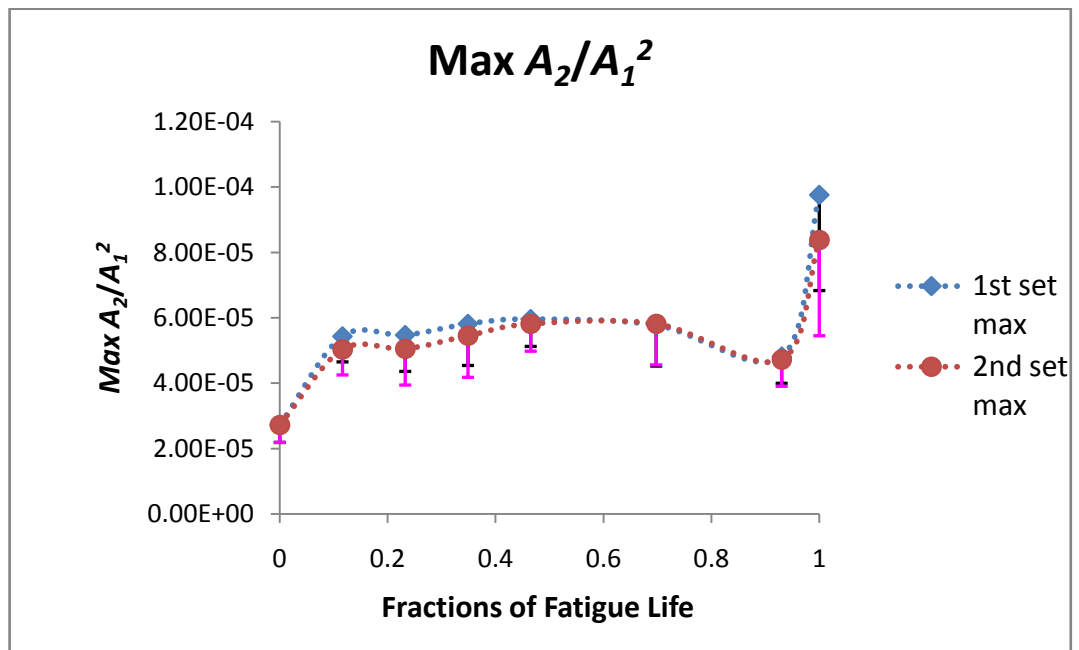


Figure 24 Variation of slope of  $A_2$  v/s  $A_1^2$  as a function of fraction of fatigue life of the sample in high amplitude regime.

**Table 5 Percentage increase in the maximum value of  $A_2/A_I^2$  at different stages of fatigue life for both the sets of the specimens in high amplitude regime**

Percentage of life	1st set max (in 1E-5)	Percentage increment	2nd set max (in 1E-5)	Percentage increment
0	2.73	0	2.70	0
0.12	5.44	99.1	5.04	84.5
0.23	5.47	100.5	5.05	85.1
0.35	5.82	113.1	5.45	99.8
0.47	5.96	118.4	5.82	113.1
0.70	5.78	111.8	5.82	113.1
0.93	4.82	76.5	4.73	73.2
1	9.76	257.6	8.38	207.02

### 3.6.2 LOW AMPLITUDE REGIME

NLU experiments in low amplitude regime were performed for all the specimens fabricated along with the high amplitude regime NLU experiments. As discussed earlier the nonlinearity parameter shows anomalous behavior for given low input amplitude due to the confinement of dislocations in three consecutive planes which results in increment of dislocation loop length by large amount.

Figure 25 shows the anomalous behavior of  $A_2/A_I^2$  in low amplitude regime for as received sample. Such figures are plotted for all the specimens considered for the experimental analysis.  $A_2/A_I^2$  at the lowest input amplitude is taken as a measure of nonlinearity parameter in this part of study.

Figure 26 shows the variation of the maximum values of  $A_2/A_I^2$  as a function of fraction of fatigue life of the specimen. The error bars shows the variation of Max  $A_2/A_I^2$

across the gauge length of the specimen. The blue line curve represents the first set whereas the red curve represents the second set.

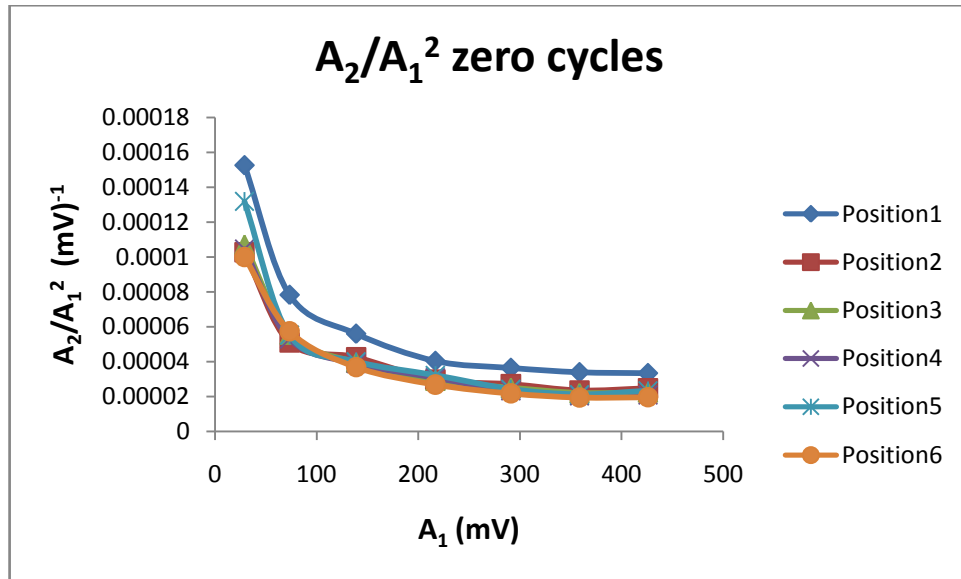


Figure 25 The anomalous behavior of  $A_2/A_1^2$  in low amplitude regime for un-fatigued sample.

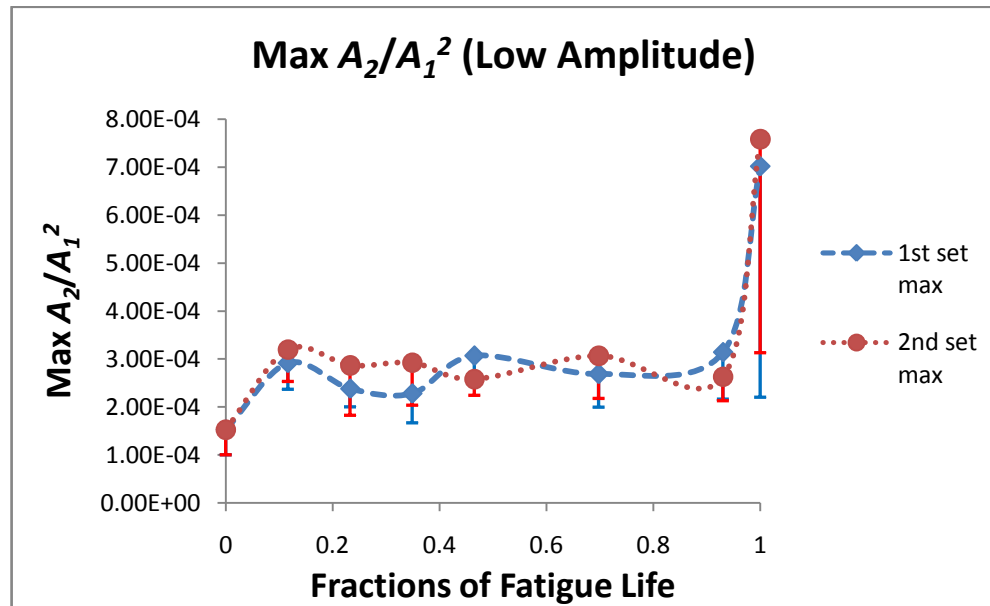


Figure 26 The variation of the maximum values of  $A_2/A_1^2$  as a function of fraction of fatigue life of the specimen in low amplitude regime

**Table 6 Percentage change of  $A_2/A_1^2$  at different stages of fatigue life in low amplitude regime**

<b>Percentage of life</b>	<b>1st set max (in 1E-4)</b>	<b>Percentage Increment</b>	<b>2nd set max (in 1E-4)</b>	<b>Percentage Increment</b>
<b>0</b>	<b>1.53</b>	<b>0</b>	<b>1.53</b>	<b>0</b>
<b>0.12</b>	<b>2.92</b>	<b>91.2</b>	<b>3.20</b>	<b>113.0</b>
<b>0.23</b>	<b>2.38</b>	<b>56.1</b>	<b>2.87</b>	<b>91.1</b>
<b>0.35</b>	<b>2.28</b>	<b>49.7</b>	<b>2.92</b>	<b>94.7</b>
<b>0.47</b>	<b>2.58</b>	<b>69.1</b>	<b>3.07</b>	<b>104.5</b>
<b>0.70</b>	<b>2.69</b>	<b>76.1</b>	<b>3.07</b>	<b>104.4</b>
<b>0.93</b>	<b>2.63</b>	<b>72.3</b>	<b>3.14</b>	<b>109.4</b>
<b>1</b>	<b>7.02</b>	<b>360.2</b>	<b>7.58</b>	<b>405.5</b>

Table 6 shows the percentage increase in the maximum value of  $A_2/A_1^2$  at different stages of fatigue life from unfatigued stage for both the sets of the specimens in low amplitude regime. The increment of nonlinearity parameter at the fractured specimen is found to be more than 350 percent.

### **3.7 Transmission Electron Microscopy (TEM) ANALYSIS**

TEM analysis was carried out for samples to look in to the microstructural changes in the material due to fatigue damage. Samples fatigued for 0%, 47% and 100% fatigue life were chosen for TEM analysis. Using wire cutting thin films of 1mm thickness were cut from the samples. The films were taken from the area of the sample which showed the highest nonlinearity across the gauge length. Location no. 3, 5 and 4 were chosen on the gauge length for the sample fatigued for 0%, 47% and 100% fatigue life respectively. The film of thickness 1mm was thinned to 100 microns by fine emery papers of grade

1/0, 2/0 and 3/0. This was further thinned to 100 angstroms by jet material removing process and used for TEM analysis.

Pure polycrystalline copper is a wavy glide FCC metal. In cyclic fatigue material is loaded and unloaded cyclically resulting in recrystallization and recovery of the material due to local increase in temperature. Material always tries to achieve the lowest possible energy state. There exist screw and edge dislocations in the material in its as received state which gets piled up against any obstacle which may be grain boundary, sub-boundary, cell wall etc. These dislocations moves from one plane to another via cross slip as the strain, resulting from applied stress, increases. These dislocations will form the possible low energy dislocation substructures at any stage of fatigue.

The sample, as received, is found to have only the pileups near the grain boundary and distributed in other regions. Figure 27 and Figure 28 show the dislocation pile-up near the grain boundary and distributed dislocations away from the grain boundary.

As the no. of fatigue cycle increases, strain in the material will increase and these dislocations will start moving as well as new dislocations will be formed. This increase in dislocation density gives rise to tangling of the dislocations and formation of dislocation cluster. According to Wilsdorf (1997), tangling is caused by the interaction of super-saturated vacancies with dislocations at the end of their glide path.

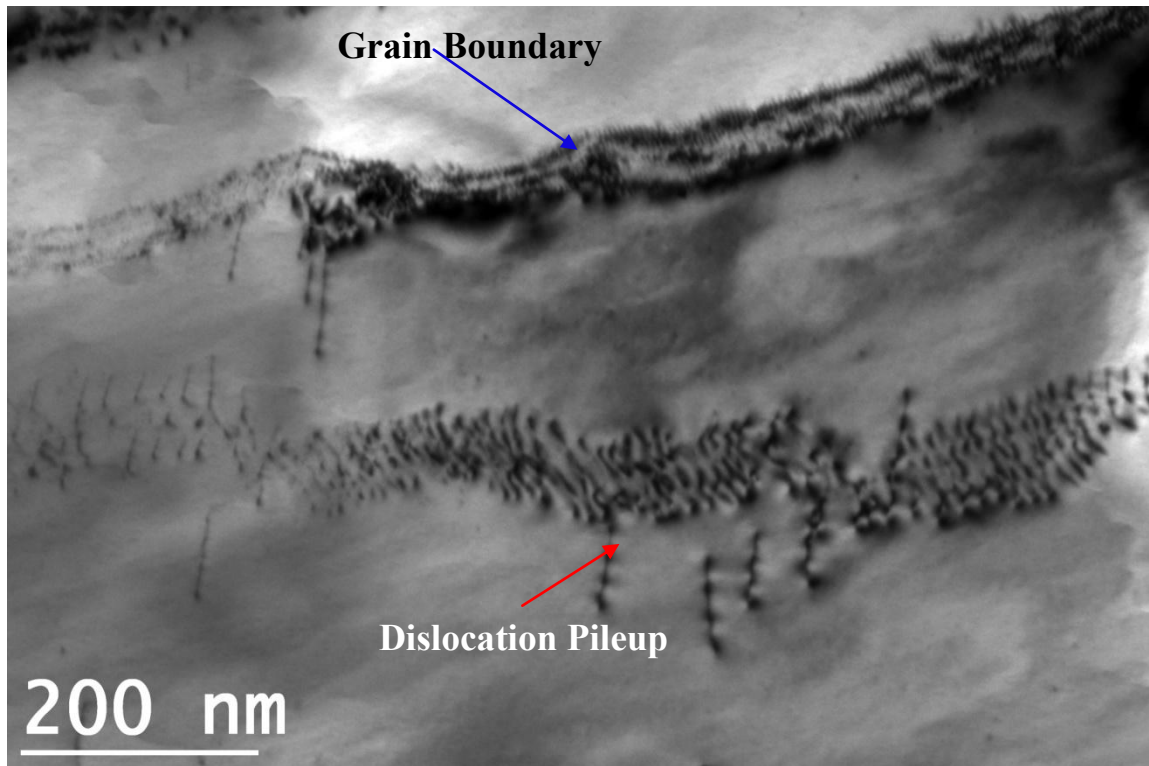


Figure 27 Dislocation Pileup near to grain boundary in as received sample

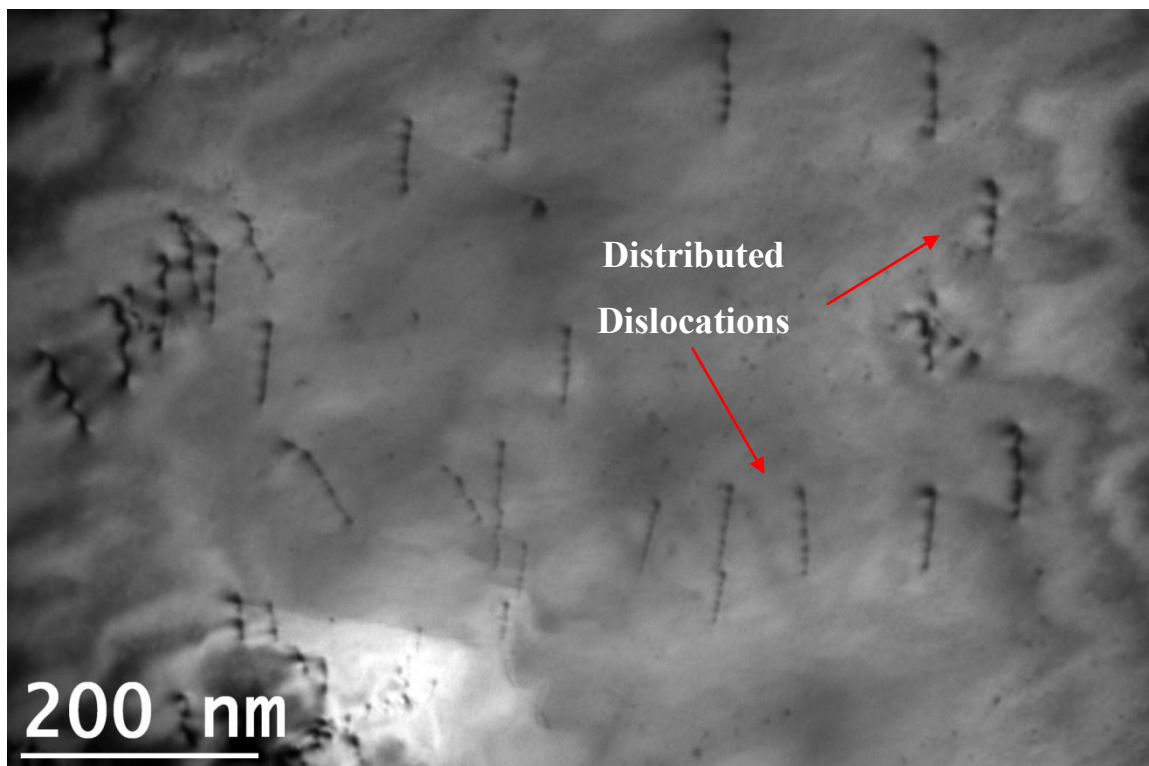


Figure 28 Distributed Individual Dislocations in as received sample

Tangling of dislocations can only be observed in wavy glide materials. Formation of dislocation bands was observed in sample fatigued for 47% of fatigue life. Figure 29 and Figure 30 show the dislocation bands and cluster of dislocations formed due to fatiguing of the material. Tangled dislocations and dislocation bands have more dislocation density than dislocation pileups but less than dislocation cell structures. Dislocation cells are surrounded by cluster dislocations and tangled dislocations with less dislocation density in the center area. Figure 31 and Figure 32 show the cell structure formed near the fracture site of the specimen which was fatigued till failure. Hikata et.al. (1965) showed from their string analogy model that nonlinearity parameter increases as the dislocation density increases. Tangling of dislocations, formation of bands and cell structure increases dislocation density which is responsible for increase in the nonlinear behavior of the material. The increase in  $A_2/A_1^2$  shown from as received state of material to various percentage of fatigue life in Figure 24 is due to increase in dislocation density in material due to fatigue loading. At the same time the increase in  $A_2/A_1^2$  at low input amplitude, as pointed out by Cantrell (2009), is due to confinement of dislocations in two adjacent planes which results in increase of dislocation loop length. The dislocations in fatigued state of the material are already locked by obstacles and other dislocations between slip planes which will make possible more loop length increment on application of small amplitude. More increase in loop length at fatigued state of the material for small input amplitude will cause larger value of  $A_2/A_1^2$  at fatigued state compared to as received state of the material which is shown in Figure 26.

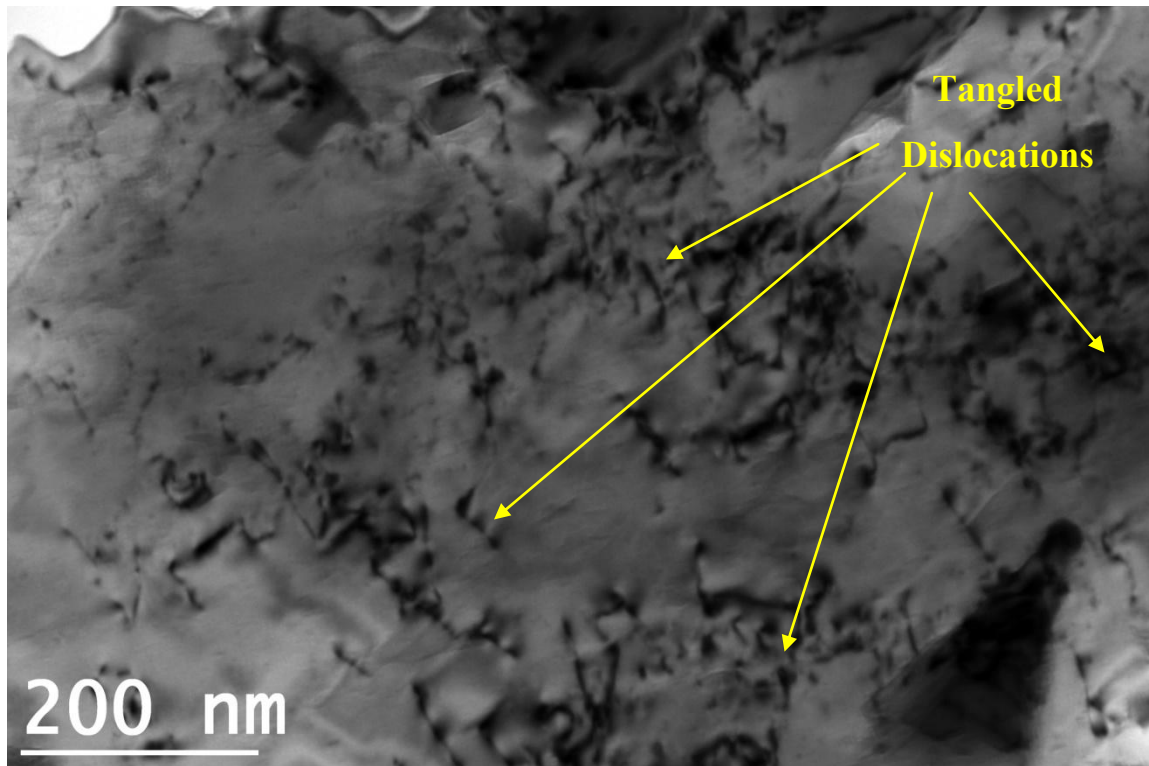


Figure 29 Tangled Dislocations in the specimen fatigued for 47% of fatigue life

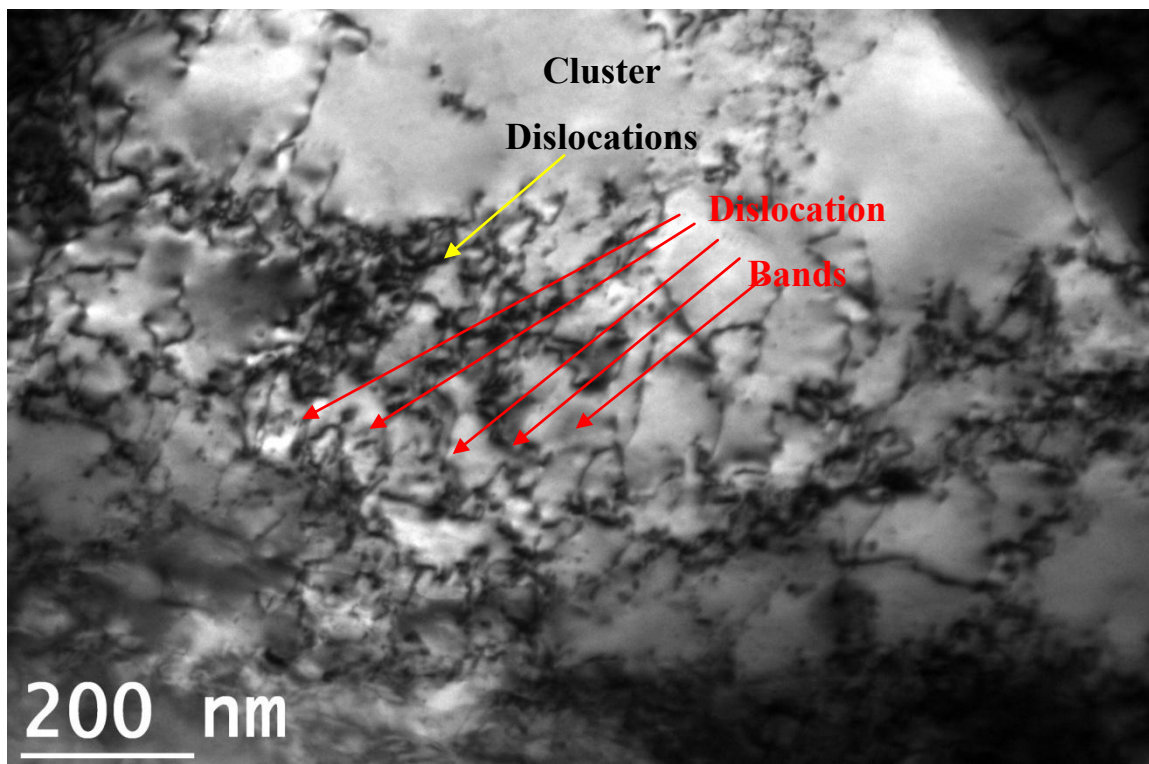


Figure 30 Dislocation Bands and Cluster dislocations in the specimen fatigued for 47% of fatigue life

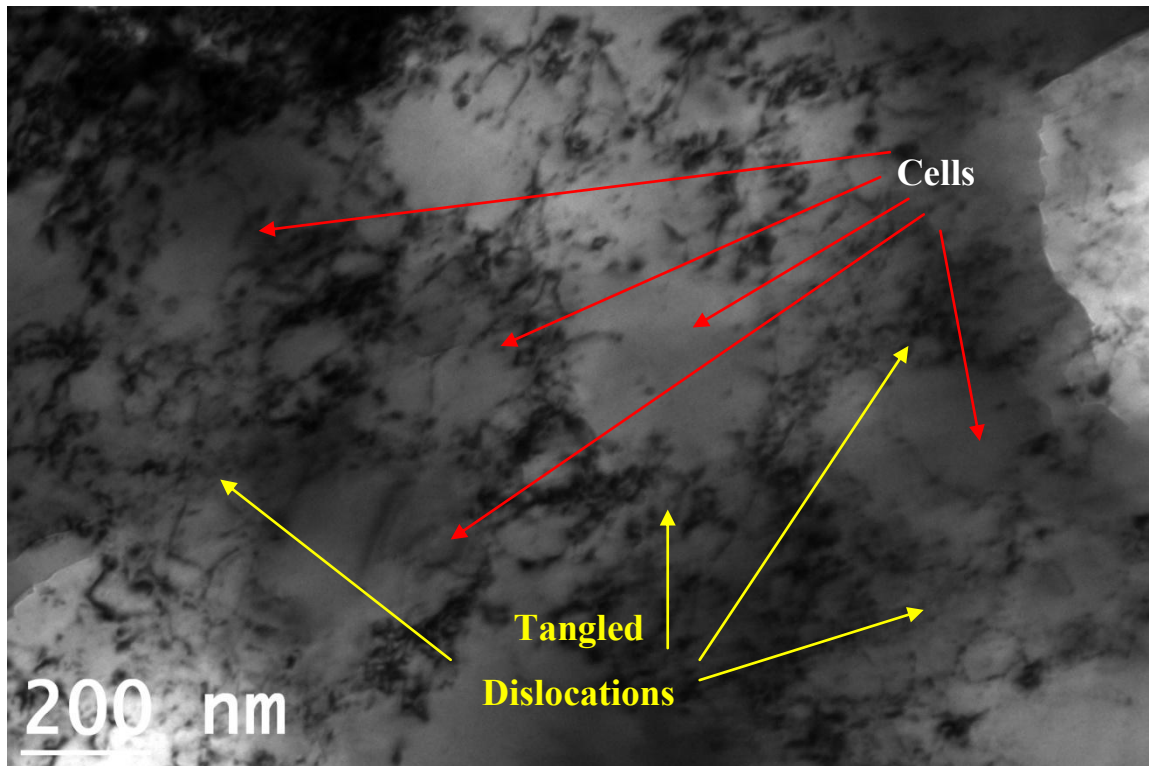


Figure 31 Cell Structure with tangled dislocations formed in completely fractured specimen

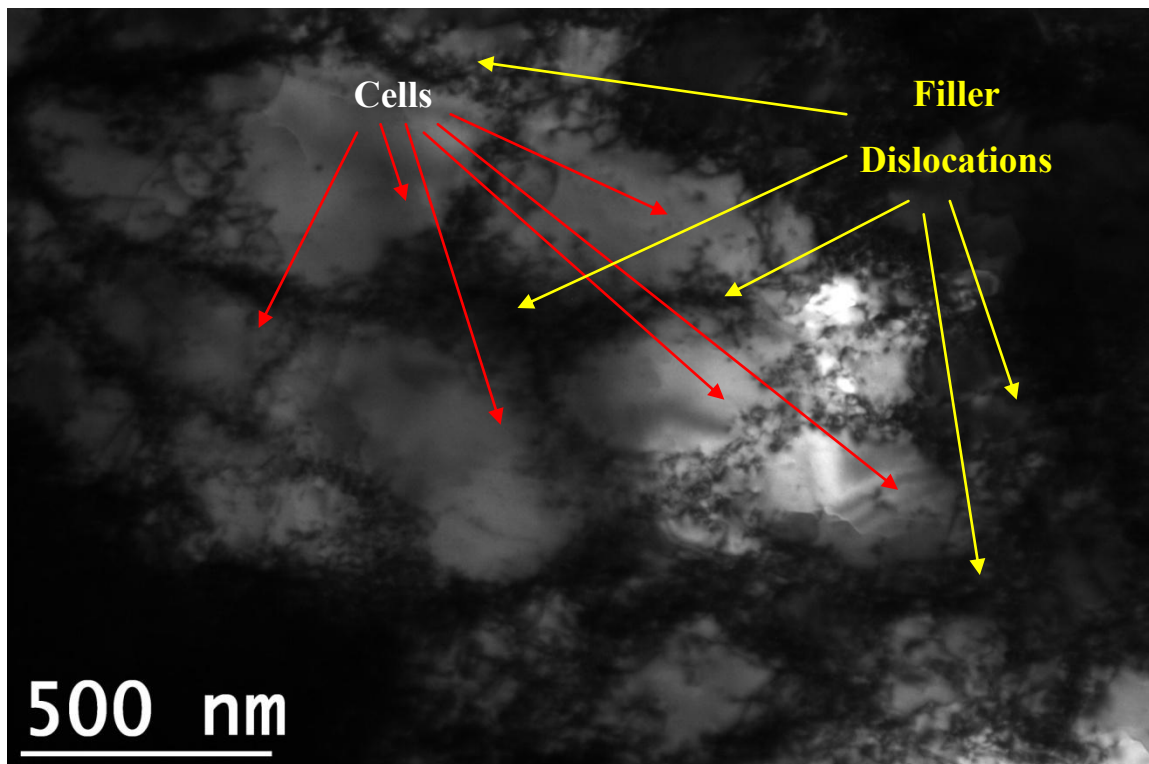


Figure 32 Cell structure in completely fractured specimen surrounded by filler dislocations

### 3.8 SUMMARY

$A_2/A_1^2$  increases as the no. of fatigue cycle increases up to 47% of fatigue life and it remains constant till 70% of fatigue life. After that it decreases till 93% of fatigue life and it shoots up near the fracture site. Similar results are obtained in low amplitude regime. Different kinds of dislocation substructures are found in TEM analysis e.g. individual dislocations, dislocation pileups, tangled dislocations, dislocation bands, and cell structures. Dislocation pileups and distributed individual dislocations have less dislocation density as compared to dislocation bands and the later have less dislocation density compared to cluster dislocations, filler dislocations, and cell structures. TEM images support the increase in  $A_2/A_1^2$  as the dislocation density increases due to increase in no. of fatigue cycles. Results showed that there was an increase of around ~250% in the nonlinear parameter  $A_2/A_1^2$  in the fatigue sample when compared to the as received sample. It was also observed that in low amplitude regime this change is ~450%.

## **4. EXPERIMENTAL DETAILS (LASER VIBROMETER RECEPTION)**

The measurement of nonlinearity of material using any experimental set will also include the systems nonlinearity in the measurement. The experimental system's nonlinearity majorly caused by contacts of transducers with material, and couplant interface. To avoid the nonlinearity caused by the couplant on receiver side the noncontact receiver can be used and laser vibrometer is a good promising transducer for capturing the various ranges of vibrations of material surface caused by propagation of longitudinal wave. As part of this work, NLU experiments were carried out to characterize the damage due to fatigue using Laser Vibrometer OFV-5000 as receiver. To simulate these damages, pure polycrystalline copper specimens were fabricated and tested on a computer controlled test system. Experimental setup of this reception technique is presented in Section 4.2.

### **4.1 CALIBRATION OF THE EQUIPMENT**

Table 7 describes the amplitude of vibrations on the face of the 5 MHz ultrasonic longitudinal transducer for a given input wave amplitude. The displacements on the face of transducer were measured by focusing the laser on directly on transducer at four different locations and the average values are presented. The variation was in experimental error of  $\pm 5\%$ . Output of the laser vibrometer in oscilloscope is recorded in mV and converted in nm by using the conversion for 5MHz frequency signal. The conversion is  $1V = 50nm$ .

**Table 7 Relationship between the RITEC power setting, the input power level to the transducer and the surface displacement as determined by the laser vibrometer for 9 cycle tone burst**

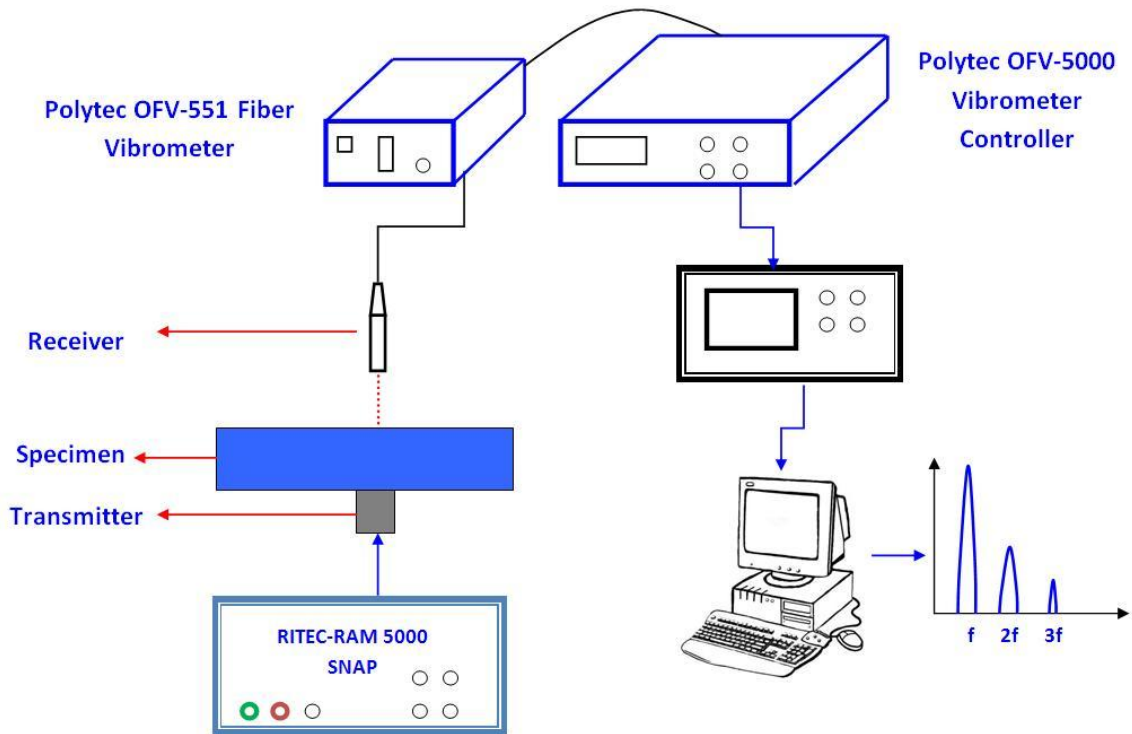
<b>RITEC Power Setting</b>	<b>Input Voltage to the Transducer (V)</b>	<b>Displacement at the face of 5MHz transducer (nm)</b>
<b>0</b>	68.4	2.78
<b>10</b>	170.5	7.59
<b>20</b>	322.1	14.98
<b>30</b>	484	23.7
<b>40</b>	646	32.56
<b>50</b>	822	41.27
<b>60</b>	990	50.23
<b>70</b>	1164	61.07
<b>80</b>	1378	74.47
<b>90</b>	1625	88.75
<b>100</b>	1880	97.93

## **4.2 EXPERIMENTAL SETUP (LASER VIBROMETER RECEPTION)**

The transmitting side in this part of study was kept as same as PZT reception. The transmitter was driven by RITEC RAM 5000 by utilizing the input control level settings. The signal was fed to the material by a PZT of central frequency 5MHz supplied by PANAMETRIC INC. The output signal was captured by laser vibrometer OFV-5000 which uses the principle of heterodyne interferometer by generating a carrier signal on the photo-detector. The beam of helium neon laser is pointed at the surface of the sample and which gets scattered back from it. The vibrating object makes frequency or phase modulation of the laser light due to the Doppler Effect. The phase modulation is used to

reconstruct the displacement signal by decoders in the laser vibrometer OFV-5000 controller.

The output signal from the controller is fed to Agilent 6032A digital Storage oscilloscope, which operates at a sampling rate of 100 MHz, for visual inspection as well as for storing the data in CSV format. For further analysis of the data, the digitized data from the oscilloscope was transferred to a USB drive with 1000 data points per window.



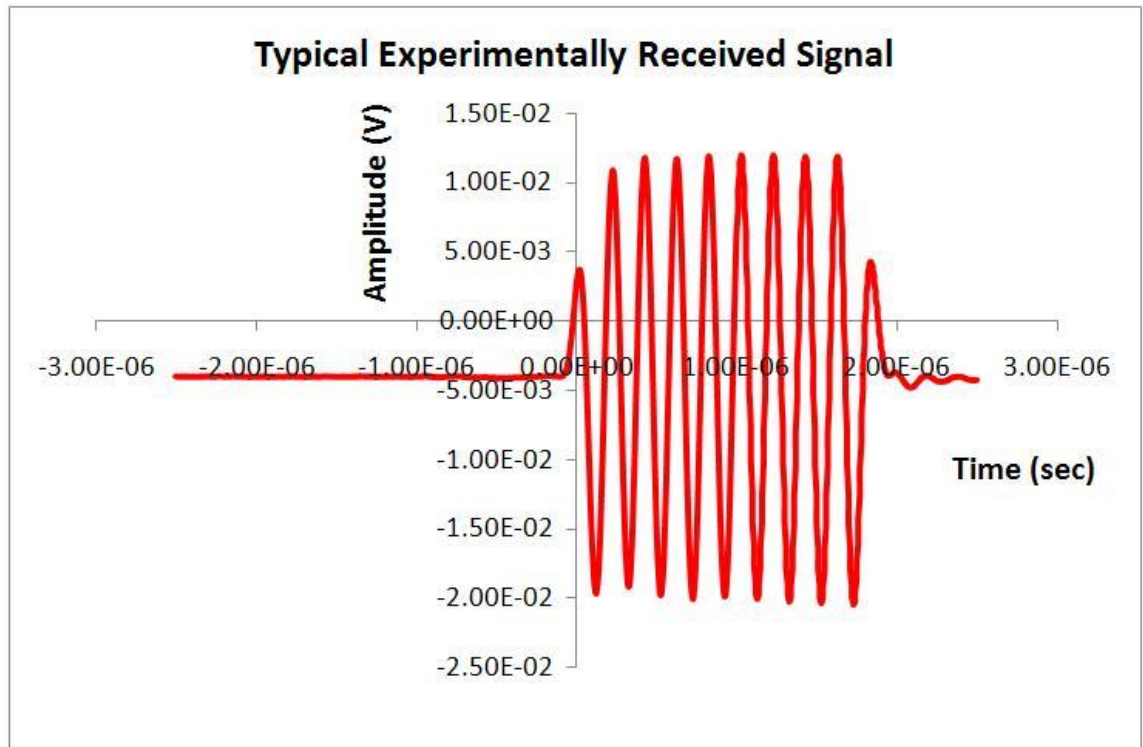
**Figure 33 Experimental setup for Laser Vibrometer Reception Technique**

Figure 33 describes the experimental setup for this part of study.

### 4.3 EXPERIMENTAL PROCEDURE

Ultrasonic transducer of diameter of 8.8 mm supplied by PANAMETRIC INC and central frequency 5 MHz was utilized as transmitter and laser vibrometer OFV-5000, supplied by POLYTEC, as receiver. In order to get a High power RF tone burst, a

RITEC RAM-5000 gated amplifier is used. On the exactly opposite side of the transmitter location the helium neon beam is pointed. As it is point detection method, the laser was pointed at four different locations for the same location of transmitter and then averaged. The output from the laser vibrometer controller is fed to an Agilent 6032A digital Storage oscilloscope, which is operating at a sampling rate of 100 MHz, for visual inspection and as well as for storing the data in CSV format. For further analysis of the data, the digitized data from the oscilloscope is transferred to a USB drive with 1000 data points per window. 50-Ohm cables were used for interconnecting different instruments that are used to minimize the losses. A typical longitudinal mode signal for sinusoidal input pulse and its Fourier transform is shown in Figure 34 and Figure 35. Coconut oil was used as the couplant between the transducer and sample.



**Figure 34 Typical Experimentally Received Signal**

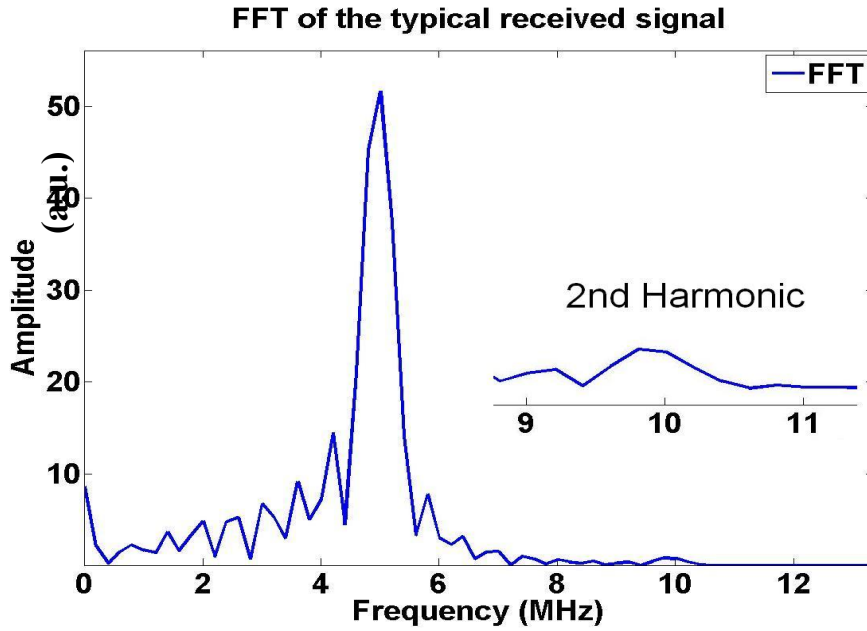


Figure 35 FFT of the Received Signal.

#### 4.4 NONLINEARITY PARAMETER FROM 2<sup>ND</sup> HARMONIC

The nonlinearity parameter is defined as

$$\beta = \frac{8A_2}{zk^2A_1^2}$$

$$A_2 = \frac{1}{8}\beta k^2A_1^2z$$



$$A_2 \propto A_1^2 \text{ for a constant } \beta$$

The expression for nonlinearity parameter indicates that for a constant  $\beta$  the second harmonic amplitude is proportional to square of the fundamental frequency amplitude.

Values of  $A_2$  and  $A_1$  are measured in volts so the nonlinearity parameter is expressed as

$A_2/A_1^2$  (slope of  $A_2$  v/s  $A_1^2$  curve). Figure 36 shows the plot of  $A_2$  v/s  $A_1^2$  for zero cycle fatigued sample.

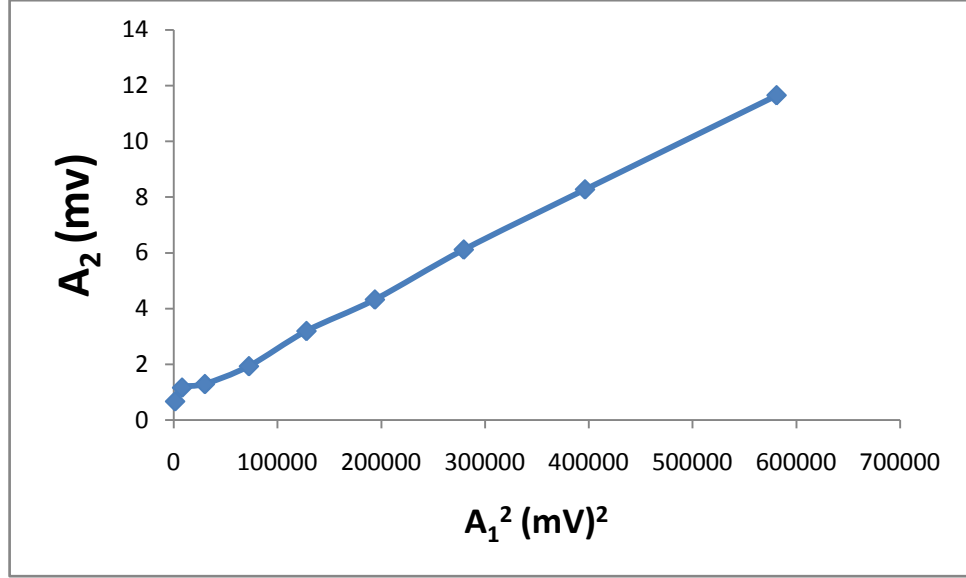


Figure 36 Plot of  $A_2$  v/s  $A_1^2$  as received sample for different locations on the sample gauge length

The slope of the lines  $A_2$  v/s  $A_1^2$  is measured at only one position on the gauge length where PZT experiment showed maximum nonlinearity. At the exactly opposite side of that particular position of transmitter the helium neon beam is pointed. As it is point detection method, the laser was pointed at four different locations for the same location of transmitter. The measurement of  $A_1$  and  $A_2$  are done five times at focusing point of laser and their overall average values have been taken for further analysis.

#### 4.5 $A_2/A_1^2$ AT LOW AMPLITUDES

As described by Cantrell (2009), there exists anomalous behavior of nonlinearity parameter at low input amplitudes. The nonlinearity parameter shows a very high value as compared to the high amplitude regime due to increase in dislocation loop length at this

stage. In this experimental study, it was found that the quantity  $A_2/A_1^2$  obtains a very high value at low input amplitudes as compared to high input amplitudes. Figure 37 shows the anomalous behavior of  $A_2/A_1^2$  as a function of input amplitude for sample which is fatigued for zero cycles. Such plots are plotted for all three samples.

The value of  $A_2/A_1^2$  at lowest possible input amplitude has been considered another representative of nonlinearity parameter.

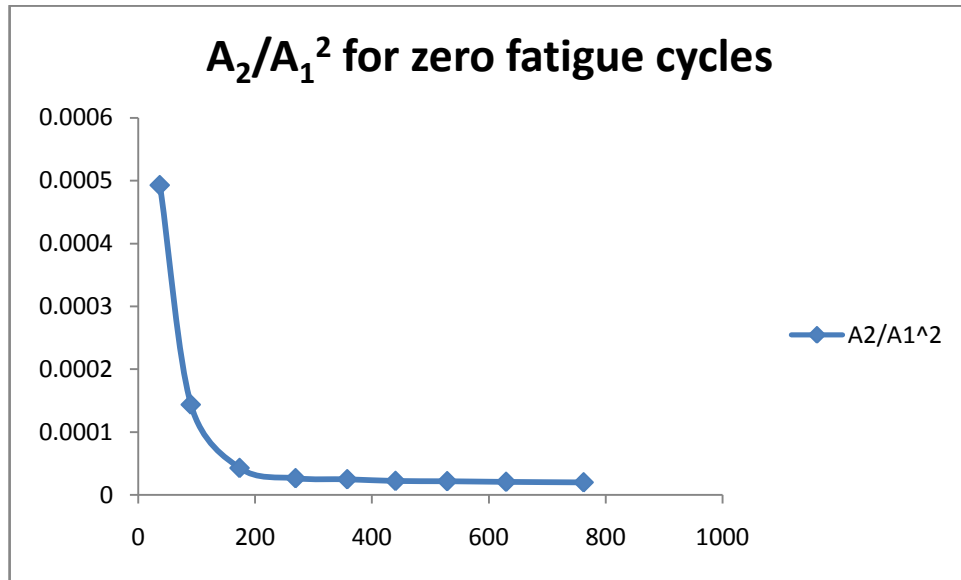


**Figure 37 The anomalous behavior of  $A_2/A_1^2$  as a function of input amplitude for zero cycle fatigued sample**

## 4.6 RESULTS

In this part of study LDV was used as the receiving transducer. Three samples, fatigued up to 0%, 47% and 93%, were chosen out of the samples considered for previous study. The signals were received only at the positions on gauge length which showed maximum value of nonlinearity parameter in PZT reception method.

Figure 38 shows the variation of  $A_2/A_1^2$  as a function of fatigue life. The  $A_2/A_1^2$  is found to increase by 300 percent from virgin state.

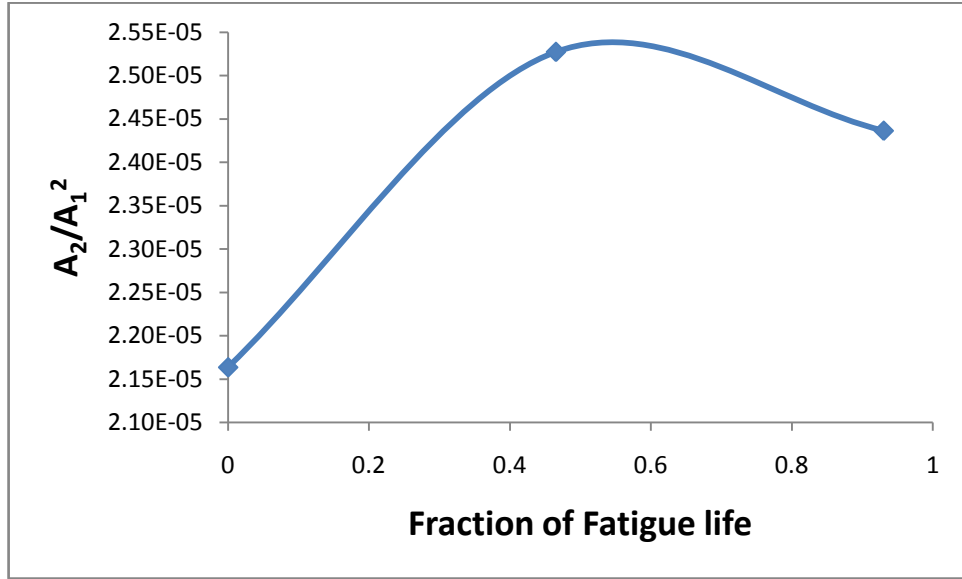
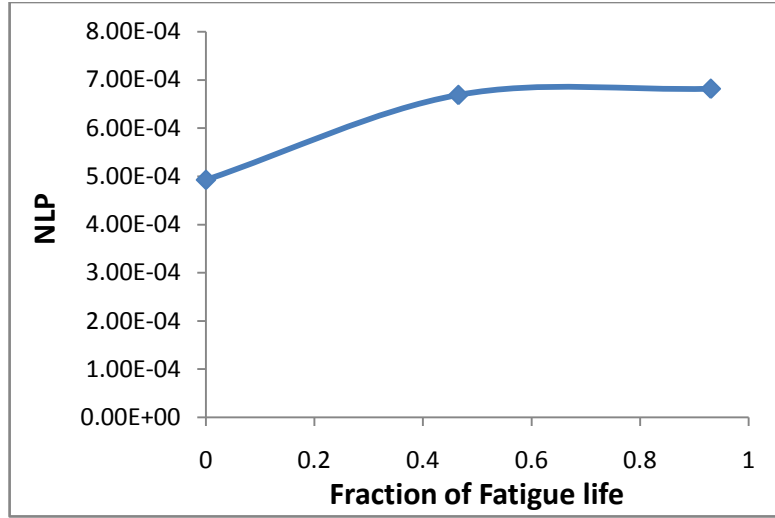


Figure 38 The variation of  $A_2/A_1^2$  as a function of fatigue life for LDV reception

$A_2/A_1^2$  at the lowest input amplitude is taken as a measure of nonlinearity parameter in this part of study.

Figure 39 shows the variation of the maximum values of  $A_2/A_1^2$  as a function of fraction of fatigue life of the material in low amplitude regime.

Table 8 shows the percentage increase in the maximum value of  $A_2/A_1^2$  at different stages of fatigue life from un-fatigued stage for both amplitude regimes.  $A_2/A_1^2$  shows an increment of 36.2 and 30.3 percent from the virgin state of the material for samples fatigued up to 47% and 93% of fatigue life respectively in high amplitude regime whereas in the low amplitude regime this percentage increment is 35.7% and 38.3%.



**Figure 39** The variation of the maximum values of  $A_2/A_1^2$  as a function of fraction of fatigue life of the material in low amplitude regime

**Table 8** The percentage increase in the maximum value of  $A_2/A_1^2$  at different stages of fatigue life from un-fatigued stage for both amplitude regimes in Laser Vibrometer reception technique

Fraction of Fatigue life	A2 v/s A1 <sup>2</sup> (LDV) (in E-05)	Percentage increment	A2/A1 <sup>2</sup> LA (LDV) (in E-04)	percentage increment
0	1.88	0	4.93	0
0.47	2.56	36.17	6.69	35.74
0.93	2.45	30.32	6.82	38.36

## 4.7 COMPARISON with PZT RECEPTION METHOD

In this section the results obtained from laser vibrometer reception technique are compared with results obtained from PZT reception technique.

$A_2/A_1^2$  in both the amplitude regimes shows the similar trend for both type of reception technique but the values are different. In high amplitude regime the values obtained from PZT reception are large whereas in low amplitude regime the values obtained from laser

reception are large. Table 9 the ratio of  $A_2/A_1^2$  obtained from laser reception to PZT reception in both the amplitude regimes.

Figure 40 shows the variation of  $A_2/A_1^2$  for both types of reception techniques as a function of fraction of fatigue life in high amplitude regime.

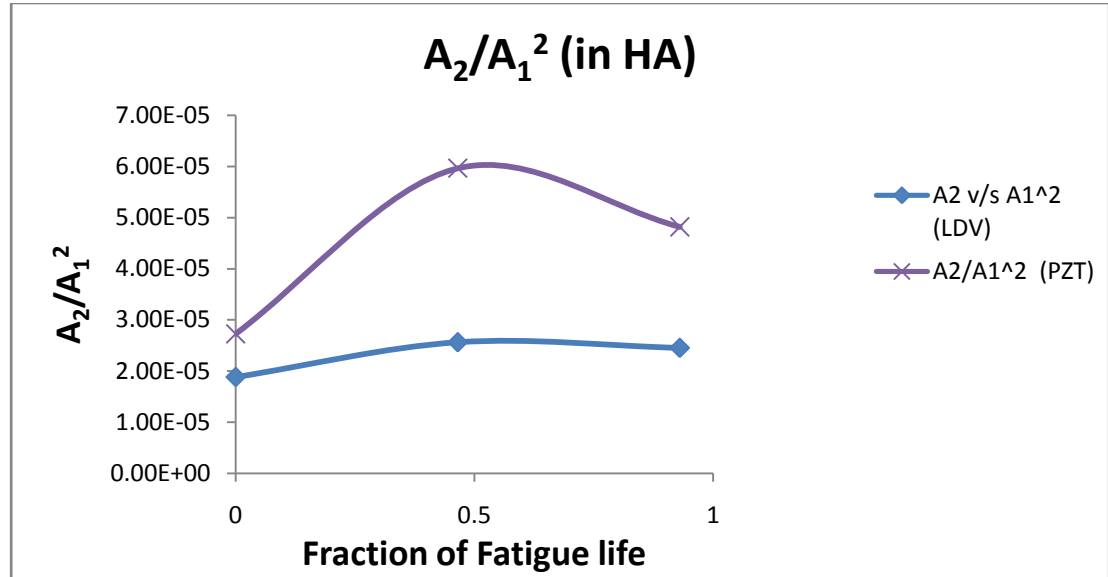


**Figure 40** The variation of  $A_2/A_1^2$  for both types of reception techniques as a function of fraction of fatigue life in high amplitude regime

Figure 41 shows the variation of  $A_2/A_1^2$  for both types of reception techniques as a function of fraction of fatigue life in low amplitude regime.

**Table 9** The ratio of  $A_2/A_1^2$  obtained from laser reception to PZT reception in both the amplitude regimes

Fraction of Fatigue life	Ratio of $A_2/A_1^2$ of Laser to PZT in HA regime	Ratio of $A_2/A_1^2$ of Laser to PZT in LA regime
<b>0</b>	0.69	3.23
<b>0.47</b>	0.43	2.59
<b>0.93</b>	0.51	2.60

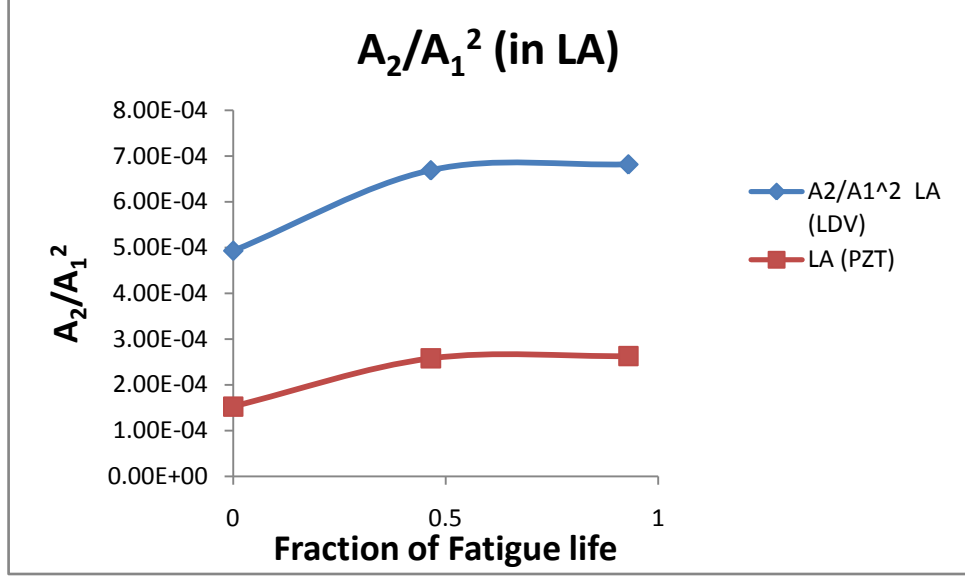


**Figure 41** The variation of  $A_2/A_1^2$  for both types of reception techniques as a function of fraction of fatigue life in low amplitude regime

#### 4.8 SUMMARY

$A_2/A_1^2$  was computed for the samples fatigued for zero%, 47% and 93% of fatigue life.  $A_2/A_1^2$  as a function of fatigue life of material is found to have similar trends for both types of reception methods, laser vibrometer as well as piezoelectric transducer, as a function of fatigue life. For high input amplitudes the  $A_2/A_1^2$  for laser vibrometer reception is 50% of the PZT reception method whereas in low amplitude regime former is approximately three times of the later.

#### 4.9 CONCLUSION

The change in reception method from PZT to laser vibrometer does not make changes in the in the trends of  $A_2/A_1^2$  as a function of fatigue life of material. The absence of couplant should reduce the captured nonlinearity at the same time presence of free surface adds nonlinearity to the system. The difference in values of  $A_2/A_1^2$  for both the reception

methods might be a function of absence of couplant and presence of free surface. This part of study requires further study with support of modeling. The thickness of the specimen plays a key role in laser vibrometer reception method and should be decided such that on-axis null does not exist on the back-wall of the specimen.

## 5. SIMULATION OF WAVE PROPAGATION IN ONE DIMENSION

This chapter deals with the simulation of the finite amplitude ultrasonic wave propagation in materials with nonlinearity. The wave propagation is simulated by solving the wave equation with the constitutive behavior of the nonlinear medium. It is proved that there should be a criterion for choosing the input parameters such as amplitude and frequency of the wave, distance of propagation for a given nonlinearity parameter. The dependencies of the generated static displacement and the second harmonic on various input parameters are evaluated and are compared with the existing literature. The simulation is carried out using finite difference time domain approach.

### 5.1 FINITE DIFFERENCE IN TIME DOMAIN

Finite-Difference Time-Domain (FDTD) is a popular modeling technique. It is easy to understand, easy to implement in software, and since it is a time-domain technique it can cover a wide frequency range with a single simulation run.



**Figure 42 One Dimensional Chain in FDTD**

Figure 42 shows the one dimensional medium where the mass is concentrated on nodes and are connected by springs having linear spring constant i.e.  $F=kx$ . The wave equation followed by the material would be

$$\rho \frac{\partial^2 y}{\partial t^2} = E \frac{\partial^2 y}{\partial x^2} \text{ or } \rho \ddot{y} = E y''$$

Where  $y$  is displacement of the node,  $x$  is direction of propagation of wave and  $t$  is time. The spatial and time derivatives are approximated using central difference scheme.

$$\ddot{y} = \frac{\partial^2 y}{\partial t^2} = \frac{y(i, k+1) - 2y(i, k) + y(i, k-1)}{dt^2} \quad (3.1.1)$$

$$y'' = \frac{\partial^2 y}{\partial x^2} = \frac{y(i+1, k) - 2y(i, k) + y(i-1, k)}{h^2} \quad (3.1.2)$$

$$y' = \frac{\partial y}{\partial x} = \frac{y(i+1, k) - y(i-1, k)}{2h} \quad (3.1.3)$$

Where  $h$  and  $dt$  are steps in space and time domain respectively and  $i$  and  $k$  are indices in space and time domain.

For stability, Courant criteria was used

$$\frac{dt}{h} \sqrt{\frac{E}{\rho}} \leq 1 \quad (3.1.4)$$

## 5.2 ONE DIMENSIONAL NONLINEAR CHAIN

In experiments material is kept between two PZT transducers. To simulate the experimental environment, PZT are considered linear medium and the material is modeled as nonlinear medium. Same impedance is chosen as couplant is used in experiments not to have impedance mismatch. So, the simulations were carried out for a chain in which the nonlinear material is surrounded by linear material of same impedance. The connections of two adjacent nodes in the linear region will follow the following equation.

$$\rho \frac{\partial^2 y}{\partial t^2} = E \frac{\partial^2 y}{\partial x^2}$$

Whereas the wave equation in the nonlinear region will be

$$\rho \frac{\partial^2 y}{\partial t^2} = E \frac{\partial^2 y}{\partial x^2} (1 - \beta \frac{\partial y}{\partial x})$$

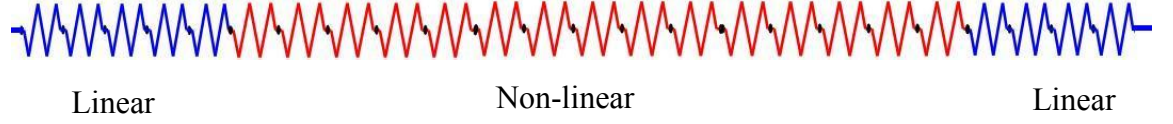


**Figure 43 One Dimensional Nonlinear Chain considered for the Simulations**

The source of excitation was kept in the linear region on the left hand side and it was made sure that the pulse will not reach the left boundary during the time of excitation. The output was received in the linear region on the right hand side and it was made sure that the pulse will not reach the right boundary before leaving the receiver completely to avoid the boundary effects.

### 5.3 SIMULATION DETAILS

The nonlinear wave equation is discretised using FDTD scheme for simulating the wave propagation in nonlinear material. The simulations are done for one dimensional case. The material is assumed to be concentrated at nodes of the chain which are connected to each other by springs having nonlinear spring constant.

The following are the terms used in the derivation

$y$ = displacement of the particle at the  $i^{\text{th}}$  node at time  $t$ .

$dt$  = time step

$h$ = distance between two consecutive nodes

$\rho$  = density of the material

$E$  = Modulus of elasticity of the material

$\beta$  = Second order nonlinearity parameter of the material.

$x$  = direction of propagation of wave

The nonlinear wave equation which look like

$$\rho \frac{\partial^2 y}{\partial t^2} = E \frac{\partial^2 y}{\partial x^2} \left( 1 - \beta \frac{\partial y}{\partial x} \right) \quad (3.2.1)$$

After substituting (3.1.1), (3.1.2) and (3.1.3) in (3.2.1)

$$\begin{aligned} & \rho \frac{y(i, k + 1) - 2y(i, k) + y(i, k - 1)}{dt^2} \\ = & E \frac{y(i+1, k) - 2y(i, k) + y(i-1, k)}{h^2} \left( 1 - \beta \frac{y(i+1, k) - y(i-1, k)}{2h} \right) \end{aligned} \quad (3.2.2)$$

After rearranging the terms

$$\begin{aligned} & y(i, k + 1) = 2y(i, k) - y(i, k - 1) + \\ & \frac{E dt^2}{\rho} \frac{y(i+1, k) - 2y(i, k) + y(i-1, k)}{h^2} \left( 1 - \beta \frac{y(i+1, k) - y(i-1, k)}{2h} \right) \end{aligned} \quad (3.2.3)$$

For stability, Courant criteria is used

$$\frac{dt}{h} \sqrt{\frac{E}{\rho}} \leq 1 \quad (3.2.4)$$

A 9 cycle sinusoidal toneburst was used as input to the simulations conducted using the above formulation. A Matlab® code was utilized to simulate the wave propagation using the FDTD equations discussed in this section. The simulations are verified against Cantrell's (1984) theory for generation of static displacement component.

The table 3.2.1 lists some of the important parameters required for the simulation. To satisfy the Courant's stability criteria first the step size in space is decided as less than  $\lambda/20$  then time step is computed to keep the Courant constant less than one. The time step was chosen such that the sampling frequency is more than 20 times of the central frequency of the input signal.

The values of input amplitudes were chosen on the basis of experimental values of displacement obtained at the face of 5MHz longitudinal transducer.

**Table 10 Important Parameters used in Simulation**

S. No.	Name of the Parameter	Value
1.	Step in Time Domain	5E-9
2.	Step in Space Domain	24E-6
3.	Courant Constant	0.9484
4.	Nonlinearity Parameter	30
5.	Density of Material	8920 kg/m <sup>3</sup>
6.	Young's Modulus	110G Pa
7.	No. of Pulses in Input Signal	9
8.	Frequency of the Signal	5 MHz

## 5.4 PULSE INVERSION

The static displacement component and second harmonic were calculated from pulse inversion technique as discussed in Section 1.3.

Theoretically two signals with 0 deg in-phase and 180 deg out of phase should be sent from transmitter and should be collected at the receiver. In simulation in-phase and out of phase signals were sent independently and collected at the same receiver point. After having saved two signals the average of them found out which will result the DC shifted 2<sup>nd</sup> harmonic signal in time domain. Figure 44 shows the two pulses at the receiver where the blue is in-phase and red is out-of-phase. Figure 45 shows the resultant 2<sup>nd</sup> harmonic pulse after adding the 2 pulses shown in Figure 44.

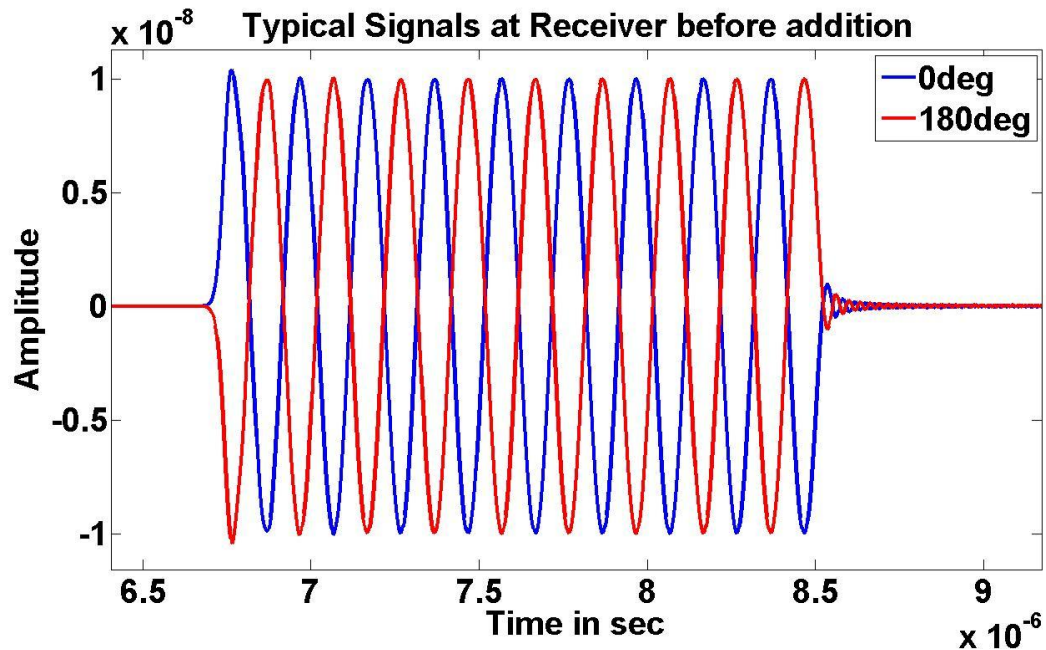


Figure 44 The two pulses at the receiver where the blue is in-phase and red is out-of-phase

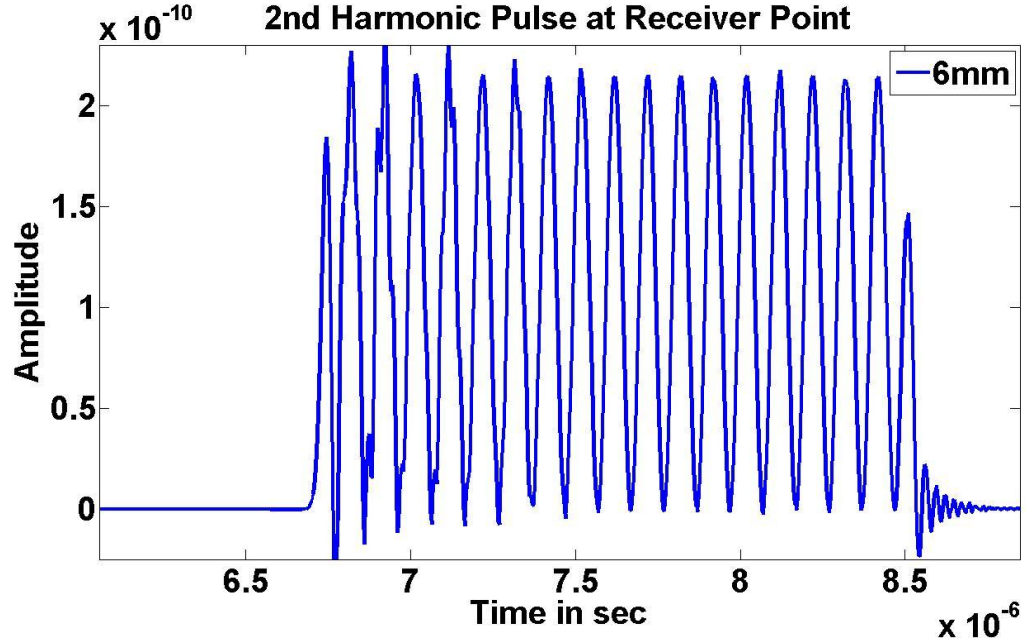


Figure 45 The resultant 2nd harmonic pulse after adding the 2 pulses shown in Figure 3

## 5.5 BOUNDARY CONDITIONS

Infinite Boundary conditions from Reynolds (1978) used in simulations are employed so that reflection is negligible from the boundaries.

The boundary conditions are as follows.

The plane wave propagating to the right will satisfy

$$\frac{1}{c} \frac{\partial u}{\partial t} + \frac{\partial u}{\partial x} = 0 \quad (3.3.1)$$

The plane wave propagating to the left will satisfy

$$\frac{1}{c} \frac{\partial u}{\partial t} - \frac{\partial u}{\partial x} = 0 \quad (3.3.2)$$

Upon discretization the right boundary node will follow

$$\frac{1}{c} \frac{u(i, t + 1) - u(i, t - 1)}{2dt} + \frac{u(i) - u(i - 1)}{dx} = 0 \quad (3.3.3)$$

Upon discretization the left boundary node will follow

$$\frac{1}{c} \frac{u(i, t + 1) - u(i, t - 1)}{2dt} - \frac{u(i + 1) - u(i)}{dx} = 0 \quad (3.3.4)$$

After rearranging the terms in (3.3.3) and (3.3.4)

At left boundary

$$u(i, t + 1) = u(i, t - 1) + c \frac{2dt}{dx} (u(i + 1) - u(i))$$

At right boundary

$$u(i, t + 1) = u(i, t - 1) - c \frac{2dt}{dx} (u(i) - u(i - 1))$$

## 5.6 DEPENDENCE OF 2<sup>ND</sup> HARMONIC AND STATIC DISPLACEMENT

As derived in section 1.2 the second harmonic amplitude can be written as

$$A_2 = \frac{1}{8} \beta k^2 A_1^2 z$$

As reported by Cantrell (1984) and Karthik et.al. (2009) the Static Displacement component can be written as

$$A_{dc} = \frac{1}{8} \beta k^2 A_1^2 z$$

The above expressions show that both amplitude of second harmonic and static displacement component are directly proportional to square of the input amplitude, nonlinearity parameter, and square of the wave-number ( $\omega/c$ ) and distance of wave propagation.

In next subsections dependence of  $A_2$  and  $A_{dc}$  on these parameters will be shown.

### 5.6.1 SQUARE OF INPUT WAVE AMPLITUDE

Figure 46 shows the variation of the second harmonic amplitude and static displacement component with the amplitude of the input wave for different distances of propagation for  $f=5MHz$  and  $\beta=30$ . From least square fit it can be seen that both varies as the square of the amplitude of the input wave for all the distances of propagation.

### 5.6.2 NONLINEARITY PARAMETER $\beta$

Figure 47 shows the variation of the second harmonic amplitude and static displacement component with the nonlinearity parameter  $\beta$  of the material for different distances of propagation for  $f=5MHz$  and  $A_I=4nm$ . It was again observed that both vary linearly with the nonlinearity parameter  $\beta$  of the material for all the distances of propagation.

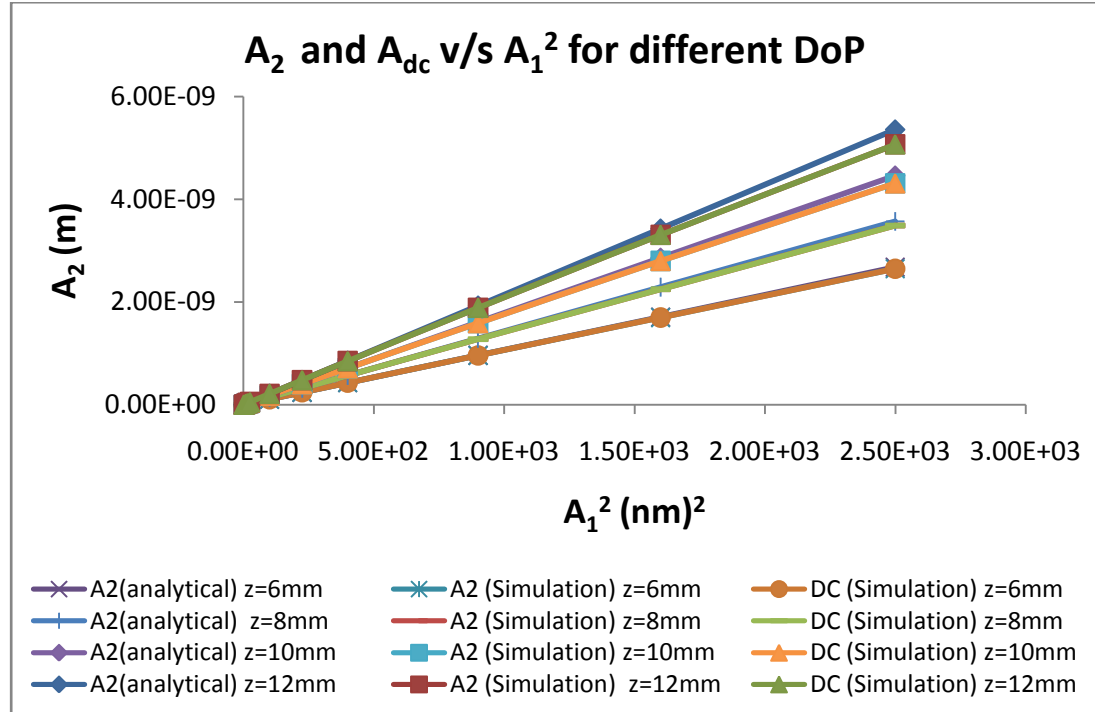
### 5.6.3 FREQUENCY OF INPUT WAVE

Figure 48 shows the variation of the static second harmonic amplitude and static displacement component with the square of frequency of the input wave for distance of propagation 6mm,  $\beta=30$  and  $A_I=4nm$ . From the least square fit it can be seen that both varies as the square of the frequency of the input wave.

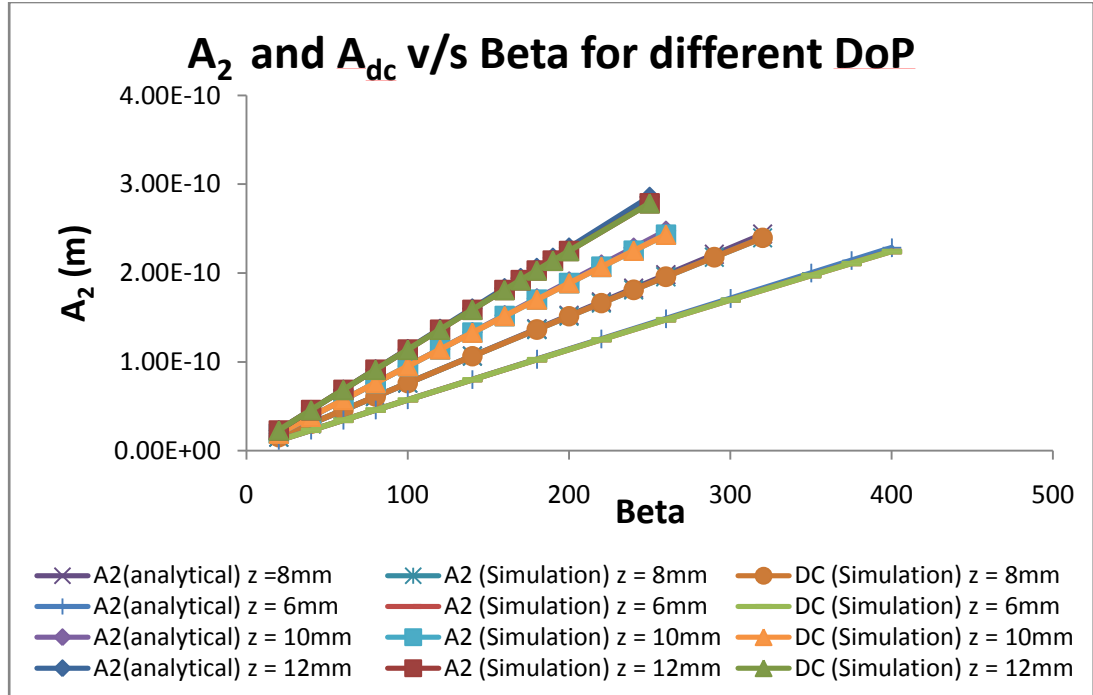
### 5.6.4 DISTANCE OF PROPAGATION

Figure 49 shows the variation of the second harmonic amplitude and static displacement component with the propagation for different Input wave amplitudes for  $\beta=30$  and

$f=5\text{MHz}$ . From the least square fit it can be seen that both varies as the square of the frequency of the input wave for input wave amplitudes.



**Figure 46 Variation of the Second Harmonic Amplitude and Static Displacement Component with the square of Amplitude of the input wave for different distances of propagation for an input wave of frequency  $f = 5\text{MHz}$ ,  $\beta = 30$**



**Figure 47 Variation of the Second Harmonic Amplitude and Static Displacement Component with the nonlinearity parameter for different distances of propagation for  $f=5\text{MHz}$ ,  $A=4\text{nn}$**

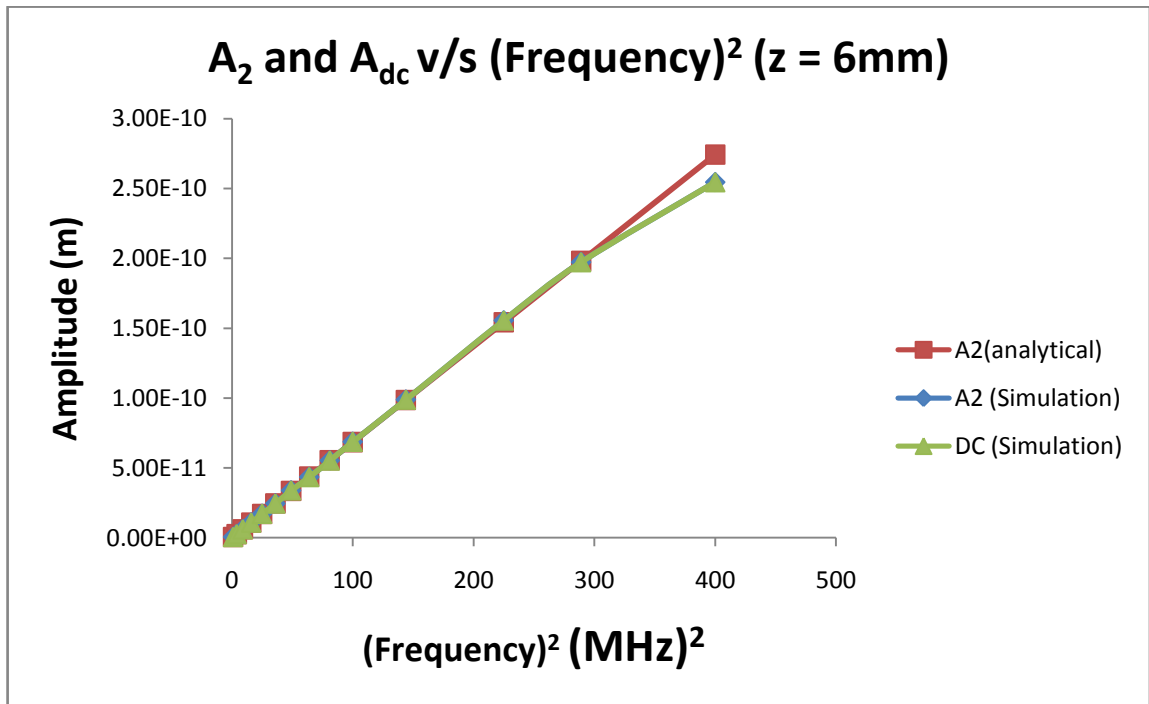


**Figure 48 Variation of the Second Harmonic Amplitude and Static Displacement Component with the square of frequency for  $z=6\text{mm}$ ,  $\beta=30$ ,  $A=4\text{nn}$**

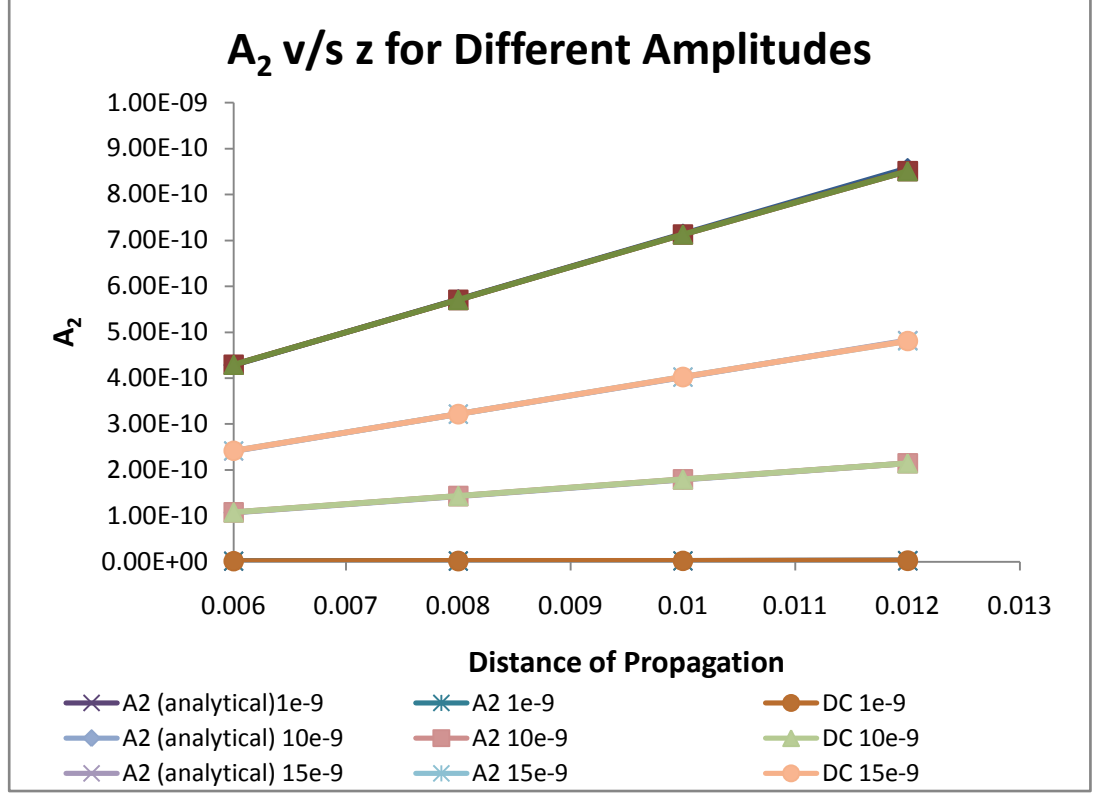


**Figure 49 Variation of the Second Harmonic Amplitude and Static Displacement Component with Distance of Propagation for different Input wave amplitudes for f=5MHz, beta=30**

## 5.7 VERIFICATION

The above results are validated against the analytical solution given in Cantrell (1984) and Thompson and Tiersten (1976).

It is found that, if  $A_2$  exceeds 5 percent of  $A_1$  then the values obtained from numerical simulation deviates from analytical values. This is shown in the following tables by marking those values in red as well as this deviation can also be seen in figures (46-49).

$$\frac{A_2}{A_1} = \frac{1}{8} \beta \frac{\omega^2}{c^2} A_1 z \leq 0.05$$

These tables are obtained by different combination of input parameters to the simulation.

**Table 11  $A_2$  as Percentage of  $A_1$  for different input wave amplitudes and distances of propagation for  $f=5\text{MHz}$   $\beta=30$**

	<b>z = 6mm</b>	<b>z = 8mm</b>	<b>z = 10mm</b>	<b>z = 12mm</b>
<b>A1 (nm)</b>	<b>(A2/A1)*100</b>	<b>(A2/A1)*100</b>	<b>(A2/A1)*100</b>	<b>(A2/A1)*100</b>
1.0	0.11	0.14	0.18	0.21
2.0	0.214	0.28	0.36	0.43
3.0	0.32	0.43	0.54	0.64
4.0	0.43	0.57	0.72	0.86
5.0	0.54	0.71	0.89	1.07
10	1.07	1.43	1.79	2.14
15	1.61	2.14	2.68	3.21
20	2.15	2.86	3.57	4.29
30	3.21	4.3	<b>5.37</b>	<b>6.43</b>
40	4.28	<b>5.73</b>	<b>7.15</b>	<b>8.58</b>
50	<b>5.36</b>	<b>7.14</b>	<b>8.92</b>	<b>10.72</b>

Table 11 shows that value of allowable  $A_1$  decreases from 40 nm to 20 nm as the distance of propagation increases from 6mm to 12mm. Similarly it can be seen from Table 3 that allowable  $\beta$  decreases from 375 to 175 as the distance of propagation increases from 6mm to 12mm whereas frequency limits itself to 17 MHz for the given material parameters.

Table 12  $A_2$  as Percentage of  $A_1$  for different values of beta and distances of propagation for  
 $f=5\text{MHz}$   $A_1=4\text{nm}$

z = 6mm		z = 8mm		z = 10mm		z = 12mm	
beta	(A2/A1)*100	beta	(A2/A1)*100	beta	(A2/A1)*100	beta	(A2/A1)*100
20	0.29	20	0.38	20	0.48	20	0.57
40	0.57	40	0.76	40	0.95	40	1.14
60	0.86	60	1.14	60	1.43	60	1.71
80	1.14	80	1.52	80	1.90	80	2.29
100	1.43	100	1.90	100	2.38	100	2.86
140	2.00	140	2.66	120	2.86	120	3.43
180	2.56	180	3.41	140	3.33	140	4.00
220	3.13	200	3.78	160	3.81	160	4.57
260	3.69	220	4.16	180	4.29	170	4.86
300	4.2	240	4.53	200	4.76	180	5.14
350	4.9	260	4.9	220	5.24	190	5.43
375	5.27	290	5.45	240	5.71	200	5.71
400	5.61	320	5.99	260	6.19	250	7.14

Table 13  $A_2$  as Percentage of  $A_1$  for different values of frequency for beta=30,  $A_1=4\text{nm}$ , z=6mm

Frequency (MHz)	(A2/A1)*100	Frequency (MHz)	(A2/A1)*100
1.0	0.017	8.0	1.09
2.0	0.068	9.0	1.38
3.0	0.15	10	1.72
4.0	0.27	12	2.47
5.0	0.43	15	3.89
6.0	0.62	17	4.93
7.0	0.85	20	6.36

## 5.8 CONCLUSION

The Nonlinear Ultrasonic experiments are meant only for small nonlinearities of the system. At large nonlinearities the approximation to neglect higher order nonlinear terms in the equation becomes questionable. One should work in a region such that the ratio of second harmonic amplitude or static displacement component to input wave amplitude should be less than 0.05. This ratio is a combination of nonlinearity parameter of the material, frequency of input wave, ultrasonic velocity of the material, input wave amplitude and distance of propagation of wave. For the values of the ratio larger than 0.05, one will be violating the assumptions taken at the time of solution of nonlinear wave equation and will end up in capturing the lesser values of nonlinearity parameter obtained from second harmonic and static displacement component. This deviation at the larger ratio might be accommodated by taking in to account the other higher order harmonic components such as 3<sup>rd</sup> and 4<sup>th</sup> order harmonic components but in present expression for overall nonlinearity parameter as a combination of nonlinearity based on static displacement, 2<sup>nd</sup> harmonic, 3<sup>rd</sup> and higher order does not exist. So, at the time of choosing the sample thickness, material and frequency of input wave one should take care of producing only small nonlinearities otherwise one will deviate from applicability region of the nonlinear equation.

## **6. DISCUSSION AND CONCLUSIONS**

Nonlinear ultrasonic harmonic generation system was used to characterize the damage due to fatigue in commercial purity (99.98%) polycrystalline copper. Dog-bone specimens for fatigue damage studies were fabricated. Through transmission experiments using longitudinal ultrasonic wave were performed to monitor NLU response at six different locations along the gage length of dog-bone sample, to ensure that NLU response close to specimen failure region is captured with fair degree of accuracy. The maximum load was 80% of the yield stress with load ratio 0.1.

Simulations were carried out to examine the applicability region of the solution nonlinear wave equation given by Tierston and Thompson (1977) and Cantrell (1984). To simulate the experimental environment one dimensional nonlinear chain embedded in two linear media of same impedance was considered. Simulations were carried out on the chain using FDTD. The second harmonic amplitude was evaluated using pulse inversion technique. Linear relationship of second harmonic amplitude and static displacement with square of input amplitude, nonlinearity parameter, square of wave number and distance of propagation were verified.

### **6.1 DISCUSSION**

Wilsdorf (1998) in his study presented that at large value of strains, formation of cell structure takes place where cells are surrounded by filler dislocations and tangled dislocations which were found in this study as shown in Figure 52. Transformation of individual dislocations and pileups into cell structure and tangled dislocations is only possible in wavy glide FCC material and polycrystalline copper is one of those. Hikata

and Elabum (1966) showed that the nonlinearity parameter is proportional to dislocation density through their model of dislocations of string analogy. As can be seen from the TEM pictures discussed in previous chapter the dislocation density has increased from virgin state to completely fatigued state of the material. The nonlinearity in material is caused by interaction of longitudinal wave propagating in the material with present dislocations, their substructures and defects. As the no. of fatigue cycles increases, as Cantrell (2004) pointed out, the dislocations present in the material forms particular types of structures starting from vein structure, PSBs and then transformation to micro-cracks and cracks takes place. Cantrell and Yost (2001) reported that micro-cracks of insufficient length do not contribute to nonlinearity. The decrease in  $A_2/A_1^2$  at 93% of fatigue life is attributed to formation of micro-cracks.

Similar loading condition were been used by Jayarao et.al. (2008) for the fatigue damage study using hourglass samples of high strength Al-Cu-Zn-Mg alloy AA7175-T7351. They also observed the decrement in nonlinearity parameter just before the fracture as shown in Figure 53. This decrease in nonlinearity parameter is assumed to be attributed to the transformation some PSBs to micro-cracks of length which are not sufficient to produce the nonlinearity.

The increase in  $A_2/A_1^2$  at low input amplitude, as pointed out by Cantrell (2009), is due to confinement of dislocations in two adjacent slip planes which results in increase of dislocation loop length. The dislocations in fatigued state of the material are already locked by obstacles and other dislocations between slip planes which will make possible more loop length increment on application of small amplitude. More increase in loop length at fatigued state of the material for small input amplitude will cause larger value

of  $A_2/A_1^2$  at fatigued state compared to as received state of the material as shown in Figure 51.

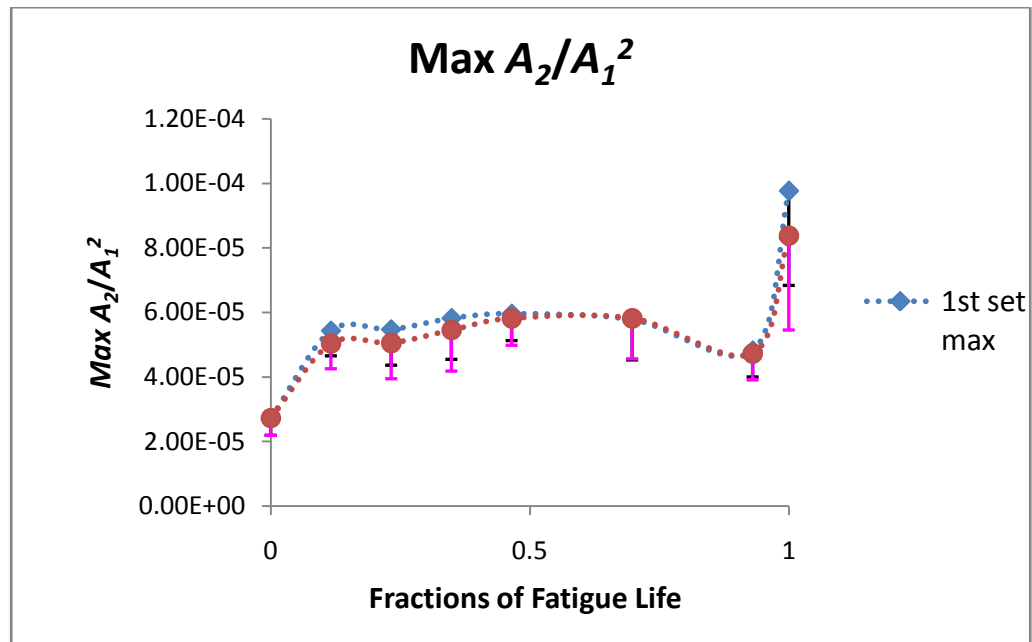


Figure 50 Variation of slope of  $A_2$  v/s  $A_1^2$  as a function of fraction of fatigue life of the sample in high amplitude regime

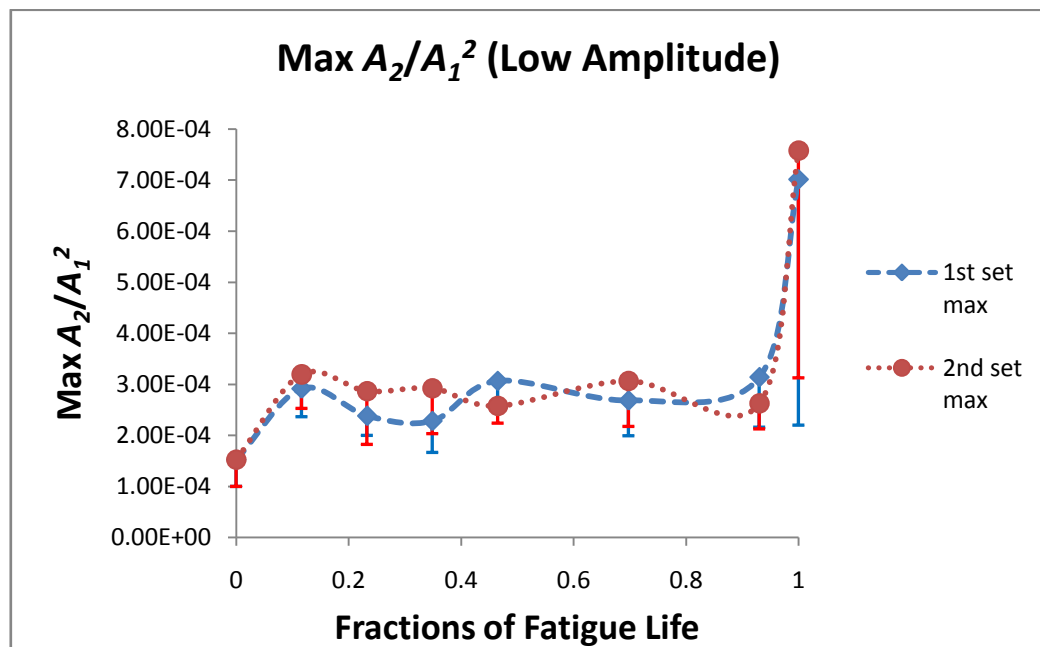


Figure 51 The variation of the maximum values of  $A_2/A_1^2$  as a function of fraction of fatigue life of the specimen in low amplitude regime

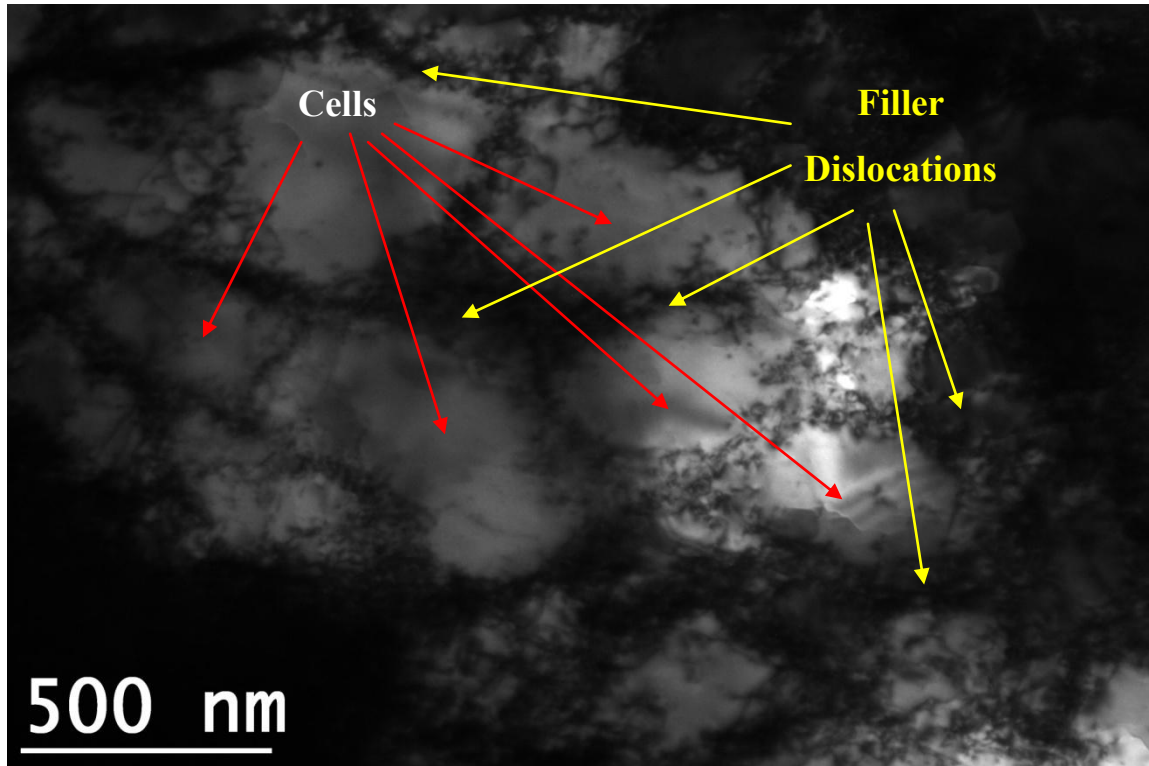


Figure 52 Filler dislocations and tangled dislocations in completely fatigued specimen

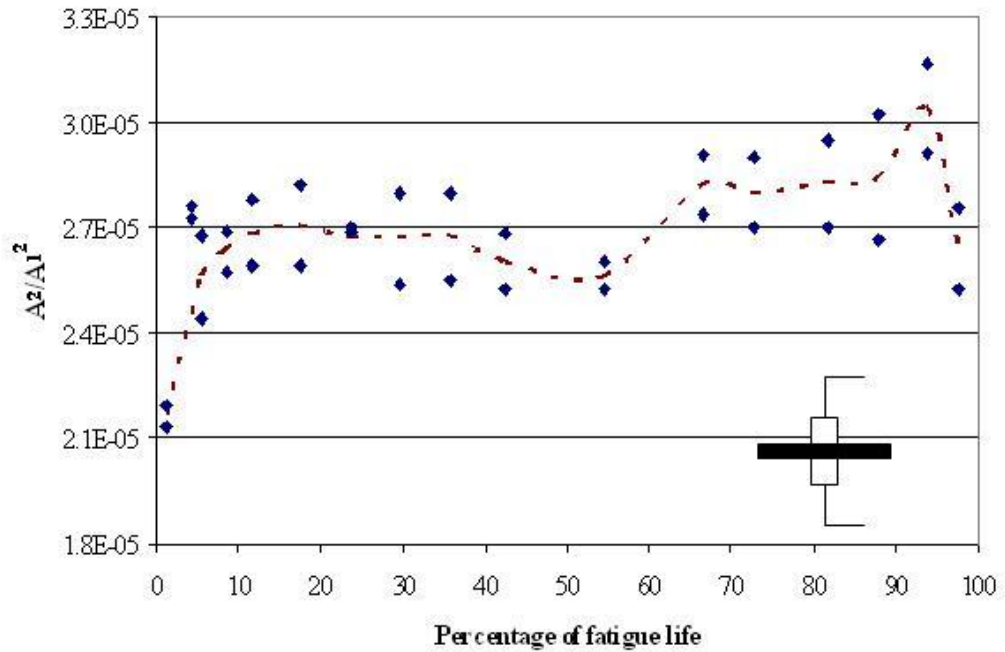


Figure 53 Variation of the longitudinal mode nonlinear parameter with the percentage of fatigue life. (Specimen fatigue loaded at 90% of yield strength).

## 6.2 CONCLUSIONS

The loading of material with increased number of fatigue cycles changes the internal structure of the material changes. This change in microstructure results in the transformation of one kind of dislocation substructure into another. Distributed and piled up dislocations transforms into tangled dislocations, dislocation bands and cell structures surrounded by filler and cluster dislocations with more density. This change, movement and generation of dislocations add nonlinearity to the material which can be seen in variation of  $A_2/A_1^2$  as a function of fraction of fatigue life.

The anomalous behavior of nonlinearity parameter at low input amplitudes has been reported before by Jayarao *et al* (2008), Karthik *et al* (2007), Balasubramaniam *et al* (communicated). The large value of nonlinearity parameter at low input amplitudes as compared to high input amplitudes is due to the confinement of dislocations into adjacent lattice planes known as quiescent lattice planes. These large values of nonlinearity parameter are in good agreement with the results obtained with high input wave amplitudes and were used for the characterization of fatigue damage in our work. This method provides an alternative low-cost technique to the high amplitude measurements that are often used for characterizing fatigue damage.

The Nonlinear Ultrasonic experiments are meant only for small nonlinearities of the system. At large nonlinearities the approximation to neglect higher order nonlinear terms in the equation becomes wrong. One should work in a region such that the ratio of second harmonic amplitude or static displacement component to input wave amplitude should be less than 0.05. This ratio is a combination of nonlinearity parameter of the material, frequency of input wave, ultrasonic velocity of the material, input wave ampli-

tude and distance of propagation of wave. For the values of the ratio larger than 0.05, one will be violating the assumptions taken at the time of solution of nonlinear wave equation and will end up in capturing the lesser values of nonlinearity parameter obtained from second harmonic and static displacement component. This deviation at the larger ratio might be accommodated by taking in to account the other higher order harmonic components such as 3<sup>rd</sup> and 4<sup>th</sup> order harmonic components.

## REFERENCES

- Balasubramaniam K., Valluri J. S., and Prakash R. V.,** Creep damage characterization using a low-amplitude nonlinear ultrasonic technique, to appear in *Materials Characterisation* (2011)
- Bermes C., Jin-Yeon K., Qu J. and Jacobs L. J.** (2007), Experimental Characterization of Material Nonlinearity using Lamb Waves, *Applied Physics Letters* 90, 021901
- Cantrell J. H.** (1984), Acoustic Radiation Stresses in Solids, *Physical Review B*, Vol. 30 Number 6
- Cantrell J. H., Jr., and Winfree W. P.,** (1984) Acoustic Radiation Stresses in Solids, *Physical Review B*, Vol. 30 Number 6,
- Cantrell J. H. and Yost W.T.,** (1997) Effect of Precipitate Coherency Strains on Acoustic Harmonic Generation, *J. Appl. Phys.*, Vol. 81, No. 7
- Cantrell J. H., and Yost W. T.,** (2001) Nonlinear Ultrasonic Characterization of Fatigue Microstructures, *International Journal of Fatigue* 23 S487–S490
- Cantrell J. H.,** (2004) Substructural Organization, Dislocation Plasticity and Harmonic Generation in Cyclically Stressed Wavy Slip Metals, *Mathematical, Physical and Engineering Sciences*, Vol. 460, No. 2043, pp. 757-780
- Cantrell J. H.,** (2006) Quantitative Assessment of Fatigue Damage Accumulation in Wavy Slip Metals from Acoustic Harmonic Generation, *Philosophical Magazine*, Vol. 86, No. 11, 1539–1554,
- Cantrell J. H.,** (2008) Effects of Diffraction and Dispersion on Acoustic Radiation Induced Static Pulses, *Applied Physics Letters* 92, 231914
- Cantrell J. H.,** (2009) Nonlinear Dislocation Dynamics at Ultrasonic Frequencies, *Journal of Applied Physics* 105, 043520,

**Hikata A., Chick B. B., and Elbaum C.,** (1965) Dislocation Contribution to the Second Harmonic Generation of ultrasonic waves, *Journal of Applied Physics* Vol. 36 Number1

**Hikata A. and Elbaum C.,** (1966) Generation of Ultrasonic Second and Third Harmonic due to Dislocations I, *Physical Review* Vol. 144 Number2

**Harumi K.,** (1986) Computer Simulation of Ultrasonics in Solids, *NDT International*. Volume 19, No. 5,

**Herrmann J., Kim J., Jacobs. L. J., Qu J., Littles J. W. and Savage M. F.,** (2006) Assessment of Material Damage in a Nickel-base Superalloy using Nonlinear Rayleigh Surface Waves, *Journal of Applied Physics* 99, 124913

**Hurley D. C., Balzar D., Purtscher P. T., and Hollman K. W.,** (1998) Nonlinear Ultrasonic Parameter in Quenched Martensitic Steels, *Journal of Applied Physics*, Volume 83, No. 9,

**Hyunjune Y. and Younghoon S.,** (2000) Numerical Simulation and Visualization of Elastic Waves Using Mass-Spring Lattice Model, *IEEE transactions on ultrasonics, ferroelectrics, and frequency control*, vol. 47, no. 3

**Jayarao V. V. S., Elankumaran K., Raghu V P., and Balasubramaniam K.,** (2008) Fatigue Damage Characterization using Surface Acoustic Wave Nonlinearity in Aluminum alloy AA7175-T7351, *Journal of Applied Physics*, 104, 1

**Jacobs L. J., Kim J. Y., Jianmin Qu, and Littles J. W.,** (2006) Experimental Characterization of Fatigue Damage in a Nickel-base Superalloy using Nonlinear Ultrasonic Waves, *J. Acoustical Society of America*. [DOI: 10.1121/1.2221557]

**Jacob X., Takatsu R., Barrière C., and Royer D.,** (2006) Experimental Study of the Acoustic Radiation Strain in Solids, *Applied Physics Letters* 88, 134111

**Karthik T. N., Elankumaran K., and Balasubramaniam K.,** (2007) Simplified Experimental Technique to Extract the Acoustic Radiation Induced Static Strain in Solids, *Applied Physics Letters* 91, 134103

**Karthik T.N., Kannan E., and Balasubramaniam K.,** (2009) Issues on the Pulse-width Dependence and the Shape of Acoustic Radiation induced Static Displacement pulses in Solids, *J. Appl. Phys.* 105, 073506

**Kommareddy V., Ramaswamy S., Ganesan B., Oruganti R., Bala R. and Shyamsunder MT,** (2006), Quantification of Fatigue using Nonlinear Ultrasound Measurements, *ECNDT - Fr.1.5.4*

**Kyung Y. J.**, (2009), Nonlinear Ultrasonic Techniques for Nondestructive Assessment of Micro-damage in Material, *International Journal of Precision Engineering and Manufacturing* Vol. 10, No. 1, pp. 123-135

**Jitendra S. V.**, (2009) Creep Damage Characterization of Material Systems using Nonlinear Acoustic Techniques, IIT Madras, Chennai, India, Master of Science *Thesis*

**Nilsson S., Petersson N. A., Sjögreen B., and Kreiss H. O.**, (2006), Accurate and Stable Finite Difference Approximations of the Elastodynamic Equations in Second order formulation, *Journal of Computational Physics*

**Peter Li, W. T. Yost, J. H. Cantrell , and K. Salama**, (1985), Dependence of Acoustic Nonlinearity Parameter on Second Phase Precipitates of Aluminum Alloys, *Ultrasonics Symposium*

**Pruell C., Jin-Yeon K., Qu J. and Jacobs L. J.**, (2007), Evaluation of Plasticity Driven Material Damage using Lamb Waves, *Applied Physics Letters* 91, 231911

**Reynolds A. C.** (1978), Boundary Conditions for the Numerical Solution of Wave Propagation Problems, *Geophysics* Vol. 43, No. 6, P. 109Y-1110

**Schroeder C. T. and Waymond R. Scott**, (1999) Finite Difference Time Domain Model for Elastic waves in the Ground, *International Society for Optical Engineering* vol. 3710 (2), pp. 1361-1372

**Sony B., Kowmudi B. N., Omprakash C. M., Satyanarayana D.V.V., Balasubramaniam K. and Kumara V.**, (2008) Creep Damage Assessment in Titanium Alloy using a Nonlinear Ultrasonic Technique, *Scripta Materialia* 59, 818–821

**Thirunavukkarasu S., Rao B.P.C., Jayakumar T., Kalyanasundaram P., Raj B. and Balasubramaniam K.**, (2002) Nonlinear Ultrasonic Method for Material Characteristics, *NDE 2002*, Proc. National Conf. of ISNT.

**Thompson R. B. and Tierston H. F.**, (1977) Harmonic Generation of Longitudinal Elastic Waves, *Journal of Acoustic Society of America*, Vol. 62, No.1

**Yost W.T. and Cantrell J. H.**, (1992) The Effects of Fatigue on Acoustic Nonlinearity in Aluminum Alloys, 1051-0117/92/0000-09 *IEEE Trans.*